Green's function representations for Marchenko imaging without up/down decomposition

Kees Wapenaar[1], Roel Snieder[2], Sjoerd de Ridder[3] and Evert Slob[1]

[1] *Department of Geoscience and Engineering, Delft University of Technology, P.O. Box 5048, 2600 GA Delft, The Netherlands*
[2] *Center for Wave Phenomena, Colorado School of Mines, Golden CO 80401, USA*
[3] *School of Earth and Environment, University of Leeds, Leeds, LS2 9JT, United Kingdom*

ABSTRACT

Marchenko methods are based on integral representations which express Green's functions for virtual sources and/or receivers in the subsurface in terms of the reflection response at the surface. An underlying assumption is that inside the medium the wave field can be decomposed into downgoing and upgoing waves and that evanescent waves can be neglected. We present a new derivation of Green's function representations which circumvents these assumptions, both for the acoustic and the elastodynamic situation. These representations form the basis for research into new Marchenko methods which have the potential to handle refracted and evanescent waves and to more accurately image steep flanks.

keywords: Controlled source seismology, Seismic interferometry, Wave scattering and diffraction

1 INTRODUCTION

Marchenko redatuming, imaging, monitoring and multiple elimination are all derived from integral representations which express Green's functions for virtual sources or receivers in the subsurface in terms of the reflection response at the surface (Ravasi et al., 2016; Staring et al., 2018; Jia et al., 2018; Lomas & Curtis, 2019; Mildner et al., 2019; Brackenhoff et al., 2019; Zhang & Slob, 2020; Elison et al., 2020; Reinicke et al., 2020). These representations, in turn, are derived from reciprocity theorems for one-way wave fields (Slob et al., 2014; Wapenaar et al., 2014), building on ideas presented by Broggini & Snieder (2012). Marchenko methods deal with internal multiples in a data-driven way and have the potential to solve large-scale 3D imaging and multiple elimination problems (Pereira et al., 2019; Staring & Wapenaar, 2020; Ravasi & Vasconcelos, 2020). Of course Marchenko methods have also limitations. One of the limitations is caused by the fact that the one-way reciprocity theorems require that the wave field in the subsurface region of interest can be decomposed into downgoing and upgoing fields. Moreover, one of these reciprocity theorems (the correlation-type theorem) is based on the assumption that evanescent waves can be neglected. These assumptions complicate the imaging of steep flanks and exclude a proper treatment of refracted waves and evanescent waves tunnelling through high velocity layers.

To address some of the limitations, Kiraz et al. (2020) propose a Marchenko method without decomposition inside the medium, assuming the input data are acquired on a closed boundary. On the other hand, for reflection data on a single horizontal boundary, a first step has been set towards a Marchenko method that deals with evanescent waves (Wapenaar, 2020). This method is restricted to horizontally layered media and uses wave field decomposition inside the medium.

In this paper we derive more general Green's function representations which do not rely on wave field decomposition in the subsurface and which hold for an arbitrarily inhomogeneous medium below a single horizontal acquisition

boundary. These representations form a starting point for new research on Marchenko methods which circumvent several of the present limitations. Diekman & Vasconcelos (2021) independently investigate the same problem, using a somewhat heuristic approach, without specifying a focusing condition for their function f. They postulate that the most compact version of f gives a proper focusing function. Our derivation follows a different approach, using an explicit focusing condition which uniquely determines our focusing function f. Moreover, we derive several forms of Green's function representations, including one for the homogeneous Green's function between a virtual source and a virtual receiver in the subsurface. We also derive elastodynamic versions of these representations.

This paper is restricted to the derivation of the Green's function representations; a discussion of their application in new Marchenko methods is beyond the scope of this paper.

2 ACOUSTIC WAVE FIELD REPRESENTATION

We consider a lossless acoustic medium, consisting of a homogeneous isotropic upper half-space and an arbitrary inhomogeneous anisotropic lower half-space, separated by a horizontal surface $\partial\mathbb{D}_R$. Coordinates in the medium are denoted by $\mathbf{x} = (\mathbf{x}_\mathrm{H}, x_3)$, with $\mathbf{x}_\mathrm{H} = (x_1, x_2)$ denoting the horizontal coordinates and x_3 the depth coordinate (the positive x_3-axis is pointing downward). The horizontal surface $\partial\mathbb{D}_R$ is defined at $x_3 = x_{3,R}$ (in the next section we choose this as the surface at which seismic acquisition takes place). The medium parameters of the lower half-space $x_3 > x_{3,R}$ are the compressibility $\kappa(\mathbf{x})$ and the mass density tensor $\rho_{jk}(\mathbf{x})$. At the micro scale (much smaller than the wavelength of the acoustic field) the mass density is isotropic. However, small-scale heterogeneities of the isotropic mass density, for example caused by fine-layering, may manifest themselves as effective anisotropy at the scale of the wavelength (Schoenberg & Sen, 1983). The mass density tensor is symmetric, that is, $\rho_{jk}(\mathbf{x}) = \rho_{kj}(\mathbf{x})$. The parameters of the upper half-space $x_3 < x_{3,R}$ are the constant compressibility $\kappa = \kappa_0$ and the constant isotropic mass density $\rho_{jk} = \delta_{jk}\rho_0$, where δ_{jk} is the Kronecker delta function. The propagation velocity of the upper half-space is $c_0 = (\kappa_0\rho_0)^{-1/2}$. At $\partial\mathbb{D}_R$ we choose the same constant isotropic medium parameters as in the upper half-space.

The basic equations for acoustic wave propagation are the linearized equation of motion

$$\rho_{jk}\partial_t v_k + \partial_j p = 0 \tag{1}$$

and the linearized deformation equation

$$\kappa\partial_t p + \partial_i v_i = q, \tag{2}$$

respectively. Here $p(\mathbf{x}, t)$ is the space ($\mathbf{x}$) and time (t) dependent acoustic pressure, $v_i(\mathbf{x}, t)$ the particle velocity and $q(\mathbf{x}, t)$ a source in terms of volume-injection rate density. Operator ∂_i stands for differentiation in the x_i-direction. Lower-case subscripts (except t) take on the values 1, 2 and 3, and the summation convention applies to repeated subscripts. Operator ∂_t stands for differentiation with respect to time. We introduce the specific volume tensor $\vartheta_{ij}(\mathbf{x})$ as the inverse of the mass density tensor, with $\vartheta_{ij}\rho_{jk} = \delta_{ik}$. Applying the operator $\partial_i\vartheta_{ij}$ to equation (1), operator ∂_t to equation (2), and subtracting the two equations yields the acoustic wave equation

$$\partial_i(\vartheta_{ij}\partial_j p) - \kappa\partial_t^2 p = -\partial_t q. \tag{3}$$

We introduce a focusing function $F(\mathbf{x}, \mathbf{x}_R, t)$, in which $\mathbf{x}_R = (\mathbf{x}_{\mathrm{H},R}, x_{3,R})$ denotes the position of a focal point at $\partial\mathbb{D}_R$, see Figure 1. For fixed $\mathbf{x}_R$ and variable $\mathbf{x}$ and t, this focusing function is a solution of wave equation (3) for the source-free situation, hence, for $q = 0$. We define the focusing property as

$$F(\mathbf{x}, \mathbf{x}_R, t)|_{x_3=x_{3,R}} \quad = \quad \delta(\mathbf{x}_\mathrm{H} - \mathbf{x}_{\mathrm{H},R})\delta(t), \tag{4}$$

and further demand that $F(\mathbf{x}, \mathbf{x}_R, t)$ is purely upgoing at $\partial\mathbb{D}_R$ and in the homogeneous isotropic upper half-space. Note that $F(\mathbf{x}, \mathbf{x}_R, t)$ is similar, but not identical, to the focusing function $f_2(\mathbf{x}, \mathbf{x}_R, t)$ introduced in Wapenaar et al. (2014). We come back to this in section 3.2.

We define the temporal Fourier transform of a space- and time-dependent function $u(\mathbf{x}, t)$ as

$$u(\mathbf{x}, \omega) = \int_{-\infty}^{\infty} u(\mathbf{x}, t)\exp(i\omega t)\mathrm{d}t, \tag{5}$$

where ω is the angular frequency and i the imaginary unit. The integral is taken from $t = -\infty$ to $t = \infty$ to account for non-causal functions, such as the focusing function $F(\mathbf{x}, \mathbf{x}_R, t)$ for which no causality condition is implied (hence,

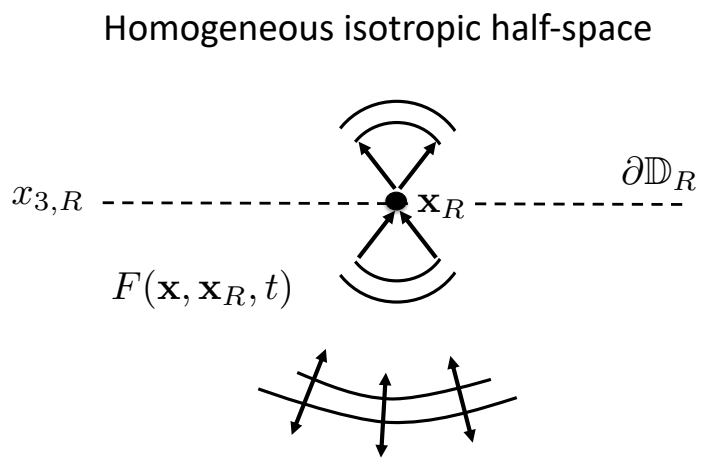

Figure 1. The focusing function $F(\mathbf{x}, \mathbf{x}_R, t)$, which focuses at $\mathbf{x}_R$. The upward pointing arrows in the upper half-space indicate that $F(\mathbf{x}, \mathbf{x}_R, t)$ is purely upgoing for $\mathbf{x}$ at and above $\partial\mathbb{D}_R$. The up/down arrows in the lower half-space indicate that $F(\mathbf{x}, \mathbf{x}_R, t)$ is a full (not decomposed) field for $\mathbf{x}$ below $\partial\mathbb{D}_R$.

in general it can be non-zero for positive and negative time). With this transform, wave equation (3) transforms to

$$Lp = i\omega q, \tag{6}$$

with

$$L = \partial_i \vartheta_{ij} \partial_j + \omega^2 \kappa. \tag{7}$$

The transformed focusing function $F(\mathbf{x}, \mathbf{x}_R, \omega)$ obeys the wave equation

$$LF = 0, \tag{8}$$

the focusing condition

$$F(\mathbf{x}, \mathbf{x}_R, \omega)|_{x_3 = x_{3,R}} = \delta(\mathbf{x}_{\mathrm{H}} - \mathbf{x}_{\mathrm{H},R}), \tag{9}$$

and it is upgoing at and above $\partial\mathbb{D}_R$. We discuss a representation for a wave field $p(\mathbf{x}, \omega)$, which may have sources in the upper half-space above $\partial\mathbb{D}_R$, but which obeys the source-free wave equation $Lp = 0$ for $x_3 \geq x_{3,R}$. In the lower half-space we express $p(\mathbf{x}, \omega)$ as a superposition of mutually independent wave fields that obey the same source-free wave equation for $x_3 \geq x_{3,R}$. For this purpose, we choose the focusing functions $F(\mathbf{x}, \mathbf{x}_R, \omega)$ and $F^*(\mathbf{x}, \mathbf{x}_R, \omega)$ (the asterisk denotes complex conjugation, which corresponds to time-reversal in the time domain). To be more specific, we express $p(\mathbf{x}, \omega)$ as

$$p(\mathbf{x}, \omega) = \int_{\partial\mathbb{D}_R} F(\mathbf{x}, \mathbf{x}_R, \omega) a(\mathbf{x}_R, \omega) \mathrm{d}\mathbf{x}_R + \int_{\partial\mathbb{D}_R} F^*(\mathbf{x}, \mathbf{x}_R, \omega) b(\mathbf{x}_R, \omega) \mathrm{d}\mathbf{x}_R, \quad \text{for} \quad x_3 \geq x_{3,R}. \tag{10}$$

Here $a(\mathbf{x}_R, \omega)$ and $b(\mathbf{x}_R, \omega)$ are yet undetermined coefficients, which depend on the position $\mathbf{x}_R$ at $\partial\mathbb{D}_R$. In Appendix A1 we formulate two boundary conditions at $\partial\mathbb{D}_R$, from which we solve $a(\mathbf{x}_R, \omega)$ and $b(\mathbf{x}_R, \omega)$. We thus obtain

$$p(\mathbf{x}, \omega) = \int_{\partial\mathbb{D}_R} F(\mathbf{x}, \mathbf{x}_R, \omega) p^-(\mathbf{x}_R, \omega) \mathrm{d}\mathbf{x}_R + \int_{\partial\mathbb{D}_R} F^*(\mathbf{x}, \mathbf{x}_R, \omega) p^+(\mathbf{x}_R, \omega) \mathrm{d}\mathbf{x}_R, \quad \text{for} \quad x_3 \geq x_{3,R}, \tag{11}$$

where $p^-(\mathbf{x}_R,\omega)$ and $p^+(\mathbf{x}_R,\omega)$ represent the upgoing ($-$) and downgoing ($+$) parts, respectively, of $p(\mathbf{x}_R,\omega)$ for $\mathbf{x}_R$ at $\partial\mathbb{D}_R$. These upgoing and downgoing fields are pressure-normalized, meaning that $p^- + p^+ = p$ at (and above) $\partial\mathbb{D}_R$. The underlying assumption in the derivation of equation (11) is that evanescent waves can be neglected at $\partial\mathbb{D}_R$. Hence, it only holds for waves which have a horizontal slowness $\mathbf{s}$ which obeys

$$|\mathbf{s}| \leq 1/c_0, \quad \text{at } \partial\mathbb{D}_R. \tag{12}$$

Note that ignoring evanescent waves at $\partial\mathbb{D}_R$ does not imply that they cannot be taken into account inside the inhomogeneous medium below $\partial\mathbb{D}_R$. For example, in an isotropic horizontally layered medium with depth-dependent velocity $c(x_3)$, in which the horizontal slowness is independent of depth, waves that are propagating at $\partial\mathbb{D}_R$ become evanescent when they reach a depth at which $1/c(x_3) < |\mathbf{s}| \leq 1/c_0$. In section 3.4 we show with a numerical example that equation (11) indeed accounts for such evanescent waves. Although for laterally varying media we cannot formulate a similar precise condition for waves becoming evanescent, it is still true that equation (11) holds for evanescent waves inside the medium, as long as they are related to propagating waves at the surface, as formulated by equation (12).

Note that we previously derived a representation similar to equation (11) with heuristic arguments, and used it as the starting point for deriving the Marchenko method (Wapenaar et al., 2013). However, further on in that derivation we applied up/down decomposition to the wave fields at an artificial internal boundary in the lower half-space and we neglected evanescent waves throughout space. In the following derivations we avoid up/down decomposition in the lower half-space and evanescent waves are only neglected at $\partial\mathbb{D}_R$. From equation (11) we derive representations for the full wave field at any point $\mathbf{x}$ in the subsurface, expressed in terms of the reflection response at the surface.

3 ACOUSTIC GREEN'S FUNCTION REPRESENTATIONS

3.1 Representation for the acoustic dipole Green's function

We introduce the Green's function $G(\mathbf{x},\mathbf{x}_S,t)$ as a solution of equation (3) for an impulsive monopole source of volume-injection rate density at $\mathbf{x}_S$, hence

$$\partial_i(\vartheta_{ij}\partial_j G) - \kappa\partial_t^2 G = -\delta(\mathbf{x}-\mathbf{x}_S)\partial_t\delta(t). \tag{13}$$

We demand that G is the causal solution of this equation, hence $G(\mathbf{x},\mathbf{x}_S,t) = 0$ for $t < 0$. Note that G obeys source-receiver reciprocity, i.e., $G(\mathbf{x},\mathbf{x}_S,t) = G(\mathbf{x}_S,\mathbf{x},t)$. In the frequency domain, $G(\mathbf{x},\mathbf{x}_S,\omega)$ obeys the following wave equation

$$LG = i\omega\delta(\mathbf{x}-\mathbf{x}_S). \tag{14}$$

We choose $\mathbf{x}_S = (\mathbf{x}_{\mathrm{H},S}, x_{3,S})$ in the upper half-space, at a vanishing distance ϵ above $\partial\mathbb{D}_R$, hence, $x_{3,S} = x_{3,R} - \epsilon$. We define a dipole-source response as

$$\Gamma(\mathbf{x},\mathbf{x}_S,\omega) = -\frac{2}{i\omega\rho_0}\partial_{3,S}G(\mathbf{x},\mathbf{x}_S,\omega), \tag{15}$$

where $\partial_{3,S}$ denotes differentiation with respect to the source coordinate $x_{3,S}$. For $\mathbf{x}$ at $\partial\mathbb{D}_R$ (i.e., just below the source) we have for the downgoing part

$$\Gamma^+(\mathbf{x},\mathbf{x}_S,\omega)|_{x_3=x_{3,R}} = \delta(\mathbf{x}_{\mathrm{H}}-\mathbf{x}_{\mathrm{H},S}). \tag{16}$$

We define the reflection response $R(\mathbf{x}_R,\mathbf{x}_S,\omega)$ of the medium below $\partial\mathbb{D}_R$ as the upgoing part of the dipole-source response $\Gamma(\mathbf{x}_R,\mathbf{x}_S,\omega)$, with $\mathbf{x}_R$ at $\partial\mathbb{D}_R$, hence

$$\begin{aligned} R(\mathbf{x}_R,\mathbf{x}_S,\omega) &= \Gamma^-(\mathbf{x}_R,\mathbf{x}_S,\omega) \\ &= -\frac{2}{i\omega\rho_0}\partial_{3,S}G^-(\mathbf{x}_R,\mathbf{x}_S,\omega) \\ &= -\frac{2}{i\omega\rho_0}\partial_{3,S}G^{\mathrm{s}}(\mathbf{x}_R,\mathbf{x}_S,\omega), \end{aligned} \tag{17}$$

where superscript s stands for scattered. Substituting $p(\mathbf{x},\omega) = \Gamma(\mathbf{x},\mathbf{x}_S,\omega)$ and $p^{\pm}(\mathbf{x}_R,\omega) = \Gamma^{\pm}(\mathbf{x}_R,\mathbf{x}_S,\omega)$ into equation (11), using equations (16) and (17), gives

$$\Gamma(\mathbf{x},\mathbf{x}_S,\omega) \quad = \quad \int_{\partial\mathbb{D}_R} F(\mathbf{x},\mathbf{x}_R,\omega)R(\mathbf{x}_R,\mathbf{x}_S,\omega)\mathrm{d}\mathbf{x}_R + F^*(\mathbf{x},\mathbf{x}_S,\omega), \quad \text{for} \quad x_3 \geq x_{3,R}. \tag{18}$$

This is a representation for the dipole response $\Gamma(\mathbf{x},\mathbf{x}_S,\omega)$ at virtual receiver position $\mathbf{x}$ anywhere in the half-space below $\partial\mathbb{D}_R$, expressed in terms of the reflection response $R(\mathbf{x}_R,\mathbf{x}_S,\omega)$ at $\partial\mathbb{D}_R$. It is similar to our earlier derived Green's function representations, but here it has been derived without applying decomposition in the lower half-space. It excludes the contribution from waves that are evanescent at $\partial\mathbb{D}_R$. A difference with our earlier representations is that the Green's function on the left-hand side is a dipole response instead of a monopole response.

3.2 Representation for the acoustic monopole Green's function

In this section we turn equation (18) into a representation for the monopole Green's function $G(\mathbf{x},\mathbf{x}_S,\omega)$. To this end we introduce a modified focusing function $f(\mathbf{x},\mathbf{x}_R,\omega)$ via

$$F(\mathbf{x},\mathbf{x}_R,\omega) \quad = \quad \frac{2}{i\omega\rho_0}\partial_{3,R} f(\mathbf{x},\mathbf{x}_R,\omega), \tag{19}$$

where $\partial_{3,R}$ denotes differentiation with respect to $x_{3,R}$. According to equations (8), (9) and (19), $f(\mathbf{x},\mathbf{x}_R,\omega)$ obeys the wave equation

$$Lf = 0, \tag{20}$$

the focusing condition

$$\partial_{3,R} f(\mathbf{x},\mathbf{x}_R,\omega)|_{x_3=x_{3,R}} \quad = \quad \frac{i\omega\rho_0}{2}\delta(\mathbf{x}_\mathrm{H} - \mathbf{x}_{\mathrm{H},R}), \tag{21}$$

and it is upgoing at and above $\partial\mathbb{D}_R$. Analogous to equations (15) and (17) we have

$$F^*(\mathbf{x},\mathbf{x}_S,\omega) \quad = \quad -\frac{2}{i\omega\rho_0}\partial_{3,S} f^*(\mathbf{x},\mathbf{x}_S,\omega). \tag{22}$$

Substituting equations (15), (17), (19) and (22) into equation (18), applying source-receiver reciprocity to the scattered Green's function and dropping the operation $-\frac{2}{i\omega\rho_0}\partial_{3,S}$ from all terms gives

$$G(\mathbf{x},\mathbf{x}_S,\omega) = \frac{2}{i\omega\rho_0}\int_{\partial\mathbb{D}_R} \{\partial_{3,R} f(\mathbf{x},\mathbf{x}_R,\omega)\} G^{\mathrm{s}}(\mathbf{x}_S,\mathbf{x}_R,\omega)\mathrm{d}\mathbf{x}_R + f^*(\mathbf{x},\mathbf{x}_S,\omega), \quad \text{for} \quad x_3 \geq x_{3,R}. \tag{23}$$

We transfer the operator $\partial_{3,R}$ from f to G^{s}, which is accompanied with a sign change (see Appendix A2). Using the definition of R in equation (17) this yields

$$G(\mathbf{x},\mathbf{x}_S,\omega) \quad = \quad \int_{\partial\mathbb{D}_R} f(\mathbf{x},\mathbf{x}_R,\omega)R(\mathbf{x}_S,\mathbf{x}_R,\omega)\mathrm{d}\mathbf{x}_R + f^*(\mathbf{x},\mathbf{x}_S,\omega), \quad \text{for} \quad x_3 \geq x_{3,R}. \tag{24}$$

This is the main result of this paper. We discuss a number of aspects of this representation.

- Equation (24) has the same form as equation (13) in Wapenaar et al. (2014), with f_2 in that paper replaced by f. Using $\partial_{3,R} f(\mathbf{x},\mathbf{x}_R,\omega) = -\partial_3 f(\mathbf{x},\mathbf{x}_R,\omega)$ for $x_3 = x_{3,R}$ (i.e., at the boundary of the homogeneous upper half-space), equation (21) can be written as

$$\partial_3 f(\mathbf{x},\mathbf{x}_R,\omega)|_{x_3=x_{3,R}} \quad = \quad -\frac{i\omega\rho_0}{2}\delta(\mathbf{x}_\mathrm{H} - \mathbf{x}_{\mathrm{H},R}). \tag{25}$$

This is the same focusing condition as that for $f_2(\mathbf{x},\mathbf{x}_R,\omega)$. The only difference between f and f_2 is the medium in which these focusing functions are defined. Focusing function f_2 is defined in a truncated version of the actual medium, where the medium below some depth level is replaced by a homogeneous medium. It is assumed that up/down decomposition is possible at the truncation level. On the other hand, focusing function f in equation (24) is defined in the actual medium (similar as F in Figure 1). In a horizontally layered medium the functions f and f_2 are identical.

Moreover, the derivation in Wapenaar et al. (2014) of the representation is different: we started with decomposed

focusing functions $f_1^+(\mathbf{x},\mathbf{x}_A,\omega)$ and $f_1^-(\mathbf{x},\mathbf{x}_A,\omega)$ in the truncated medium, with $\mathbf{x}_A$ being a focal point at the truncation depth. Next, we derived representations for $G^+(\mathbf{x}_A,\mathbf{x}_S,\omega)$ and $G^-(\mathbf{x}_A,\mathbf{x}_S,\omega)$ and combined the two into a single representation for $G(\mathbf{x}_A,\mathbf{x}_S,\omega) = G^+(\mathbf{x}_A,\mathbf{x}_S,\omega) + G^-(\mathbf{x}_A,\mathbf{x}_S,\omega)$, using the relation $f_2(\mathbf{x}_A,\mathbf{x}_R,\omega) = f_1^+(\mathbf{x}_R,\mathbf{x}_A,\omega) - \{f_1^-(\mathbf{x}_R,\mathbf{x}_A,\omega)\}^*$ (note the different order of coordinates in f_1 and f_2). The latter relation is only valid when evanescent waves can be neglected at the truncation level inside the medium. In our current approach we do not make use of decomposition at a truncation level inside the medium and we avoid the approximate relation $f_2 = f_1^+ - \{f_1^-\}^*$. The only requirement for $f(\mathbf{x},\mathbf{x}_R,\omega)$ is that it obeys equations (20) and (21). Hence, representation (24) gives the full wave field at the virtual receiver position $\mathbf{x}$ inside the medium, including multiply reflected, refracted and evanescent waves. It only excludes the contribution from waves that are evanescent at $\partial\mathbb{D}_R$, see the condition formulated by equation (12).

- Using another approach, also without applying decomposition inside the medium, Diekman & Vasconcelos (2021) derive an equation of the same form as equation (24), but without specifying a focusing condition for f. They postulate that the most compact version of their f is the focusing function. The derivation of equation (24) in the current paper uses an explicit focusing condition for f (equation 21).

- It is counterintuitive that in equation (24) we use a focusing function $f(\mathbf{x},\mathbf{x}_R,\omega)$ with its focal point $\mathbf{x}_R$ situated at the surface $\partial\mathbb{D}_R$, opposed to the focusing function $f_1^{\pm}(\mathbf{x},\mathbf{x}_A,\omega)$ in the classical representation, which has its focal point $\mathbf{x}_A$ in the subsurface. Note, however, that in the representation of equation (24) the integration takes place along $\mathbf{x}_R$, while keeping $\mathbf{x}$ fixed. Hence, in equation (24) the variable $\mathbf{x}_R$ denotes the position of Huygens sources along $\partial\mathbb{D}_R$, while $\mathbf{x}$ in $f(\mathbf{x},\mathbf{x}_R,\omega)$ plays a similar role as the focal point $\mathbf{x}_A$ in $f_1^{\pm}(\mathbf{x},\mathbf{x}_A,\omega)$.

- Equation (24) forms a starting point for deriving the Marchenko method. By applying an inverse Fourier transform we obtain

$$G(\mathbf{x},\mathbf{x}_S,t) - f(\mathbf{x},\mathbf{x}_S,-t) = \int_{\partial\mathbb{D}_R} \mathrm{d}\mathbf{x}_R \int_{-\infty}^{t} f(\mathbf{x},\mathbf{x}_R,t')R(\mathbf{x}_S,\mathbf{x}_R,t-t')\mathrm{d}t', \tag{26}$$

for $x_3 \geq x_{3,R}$. The Marchenko method is based on the separability in time of $G(\mathbf{x},\mathbf{x}_S,t)$ and $f(\mathbf{x},\mathbf{x}_S,-t)$. For horizontal plane waves in 1D media (Burridge, 1980; Broggini & Snieder, 2012) and for point-source responses at limited horizontal distances $|\mathbf{x}_\mathrm{H} - \mathbf{x}_{\mathrm{H},S}|$ in moderately inhomogeneous 3D media (Wapenaar et al., 2013), these functions only overlap at $t = t_\mathrm{d}$, which is the time of the direct arrival of the Green's function. This minimum overlap in time allows the construction of a time-windowed version of equation (26) without $G(\mathbf{x},\mathbf{x}_S,t)$ (this is the 3D Marchenko equation). From this equation the focusing function $f(\mathbf{x},\mathbf{x}_S,t)$ can be resolved, given its direct arrival and the reflection response $R(\mathbf{x}_S,\mathbf{x}_R,t)$. In essence this separability of the Green's function and the time-reversed focusing function has been the underlying assumption of all implementations of the Marchenko method. This assumption excludes, among others, the treatment of refracted waves, which may arrive prior to the direct arrival of the Green's function and interfere with the focusing function.
Since we have shown that the representations of equations (24) and (26) hold for refracted and evanescent waves, it is opportune to start new research on Marchenko methods which exploit the generality of these representations. However, in comparison with earlier developments, additional care should be taken to account for the overlap in time of the Green's function and the time-reversed focusing function. A further discussion of the development of new Marchenko methods is beyond the scope of this paper.

- Equation (24) is, in principle, suited to retrieve the Green's function $G(\mathbf{x},\mathbf{x}_S,\omega)$ for $\mathbf{x}$ anywhere in the lower half-space. However, a single type of Green's function is not a sufficient starting point for imaging. In the classical approach to Marchenko imaging, the downgoing and upgoing parts of the Green's function are retrieved, from which a reflection image can be obtained, either by a deconvolution or a correlation method. In the full-wavefield approach, we need at least one other type of field at $\mathbf{x}$, next to $G(\mathbf{x},\mathbf{x}_S,\omega)$, which represents the acoustic pressure field at $\mathbf{x}$ in response to a volume-injection rate source at $\mathbf{x}_S$. To this end we introduce a Green's function $G_i^v(\mathbf{x},\mathbf{x}_S,\omega)$ which, for i=1, 2, 3, stands for the three components of the particle velocity field at $\mathbf{x}$. From the Fourier transform of equation (1) we derive that the particle velocity v_i can be expressed in terms of the acoustic pressure as $v_i = \frac{1}{i\omega}\vartheta_{ij}\partial_j p$. Similarly, we relate G_i^v to G via

$$G_i^v(\mathbf{x},\mathbf{x}_S,\omega) = \frac{1}{i\omega}\vartheta_{ij}(\mathbf{x})\partial_j G(\mathbf{x},\mathbf{x}_S,\omega). \tag{27}$$

Hence, when $G(\mathbf{x},\mathbf{x}_S,\omega)$ is available on a sufficiently dense grid, $G_i^v(\mathbf{x},\mathbf{x}_S,\omega)$ can be obtained via equation (27). Alternatively, $G_i^v(\mathbf{x},\mathbf{x}_S,\omega)$ can be obtained from a modified version of the representation for $G(\mathbf{x},\mathbf{x}_S,\omega)$. Applying

the operation $\frac{1}{i\omega}\vartheta_{ij}\partial_j$ to both sides of equation (24) yields

$$G_i^v(\mathbf{x},\mathbf{x}_S,\omega) \quad = \quad \int_{\partial\mathbb{D}_R} h_i(\mathbf{x},\mathbf{x}_R,\omega)R(\mathbf{x}_S,\mathbf{x}_R,\omega)\mathrm{d}\mathbf{x}_R - h_i^*(\mathbf{x},\mathbf{x}_S,\omega), \quad \text{for} \quad x_3 \geq x_{3,R}, \tag{28}$$

with

$$h_i(\mathbf{x},\mathbf{x}_R,\omega) = \frac{1}{i\omega}\vartheta_{ij}(\mathbf{x})\partial_j f(\mathbf{x},\mathbf{x}_R,\omega). \tag{29}$$

The Green's functions $G(\mathbf{x},\mathbf{x}_S,\omega)$ and $G_i^v(\mathbf{x},\mathbf{x}_S,\omega)$ together provide sufficient information for imaging. For example, one could decompose the field into incident and scattered waves in any desired direction, say in a direction perpendicular to a local interface (Yoon & Marfurt, 2006; Liu et al., 2011; Holicki et al., 2019), and use these fields as input for imaging.

3.3 Representation for the homogeneous acoustic Green's function

The representations in sections 3.1 and 3.2 give the response to a source at $\mathbf{x}_S$, observed by a virtual receiver at $\mathbf{x}$ inside the medium. Here we modify this representation, to create the response at the surface to a virtual source inside the medium. After that, we show how to obtain the response to this virtual source at a virtual receiver inside the medium.

We start by renaming the coordinate vectors in equation (24) as follows: $\mathbf{x}_S \rightarrow \mathbf{x}_R$, $\mathbf{x}_R \rightarrow \mathbf{x}_S$, $\mathbf{x} \rightarrow \mathbf{x}_A$. This yields, in combination with applying reciprocity source-receiver on the left-hand side of equation (24),

$$G(\mathbf{x}_R,\mathbf{x}_A,\omega) \quad = \quad \int_{\partial\mathbb{D}_R} R(\mathbf{x}_R,\mathbf{x}_S,\omega)f(\mathbf{x}_A,\mathbf{x}_S,\omega)\mathrm{d}\mathbf{x}_S + f^*(\mathbf{x}_A,\mathbf{x}_R,\omega), \text{ for } \quad x_{3,A} \geq x_{3,R}. \tag{30}$$

Here $R(\mathbf{x}_R,\mathbf{x}_S,\omega)$ is the reflection response to a dipole source at $\mathbf{x}_S$, observed by a receiver at $\mathbf{x}_R$, both at the surface $\partial\mathbb{D}_R$. This is schematically illustrated in Figure 2(a). The integral in equation (30) describes redatuming of the sources from all $\mathbf{x}_S$ at the surface to virtual-source position $\mathbf{x}_A$ in the subsurface, see Figure 2(b). After adding $f^*(\mathbf{x}_A,\mathbf{x}_R,\omega)$ (according to equation 30)) this gives the Green's function $G(\mathbf{x}_R,\mathbf{x}_A,\omega)$, which is the response to the virtual source at $\mathbf{x}_A$, observed by the receiver at $\mathbf{x}_R$ at the surface.

Our next aim is to derive a representation for the response observed by a virtual receiver at $\mathbf{x}$ in the subsurface, given $G(\mathbf{x}_R,\mathbf{x}_A,\omega)$. Equation (11) cannot be used for this in the same way as before, since $G(\mathbf{x},\mathbf{x}_A,\omega)$ obeys a wave equation with a singularity at $\mathbf{x}_A$, whereas $p(\mathbf{x},\omega)$ in equation (11) is not allowed to have sources in the lower half-space. To overcome this problem, we define the homogeneous Green's function (Porter, 1970; Oristaglio, 1989)

$$G_\mathrm{h}(\mathbf{x},\mathbf{x}_A,\omega) = G(\mathbf{x},\mathbf{x}_A,\omega) + G^*(\mathbf{x},\mathbf{x}_A,\omega). \tag{31}$$

Here $G(\mathbf{x},\mathbf{x}_A,\omega)$ and $G^*(\mathbf{x},\mathbf{x}_A,\omega)$ obey equation (14), with source terms $i\omega\delta(\mathbf{x}-\mathbf{x}_A)$ and $-i\omega\delta(\mathbf{x}-\mathbf{x}_A)$, respectively, on the right-hand sides. Hence, $G_\mathrm{h}(\mathbf{x},\mathbf{x}_A,\omega)$ obeys the following equation

$$LG_\mathrm{h} = 0, \tag{32}$$

which confirms that the homogeneous Green's function has no singularities. This time we choose for $p(\mathbf{x},\omega)$ in equation (11)

$$p(\mathbf{x},\omega) \quad = \quad G_\mathrm{h}(\mathbf{x},\mathbf{x}_A,\omega), \tag{33}$$

with $G_\mathrm{h}(\mathbf{x},\mathbf{x}_A,\omega)$ defined in equation (31). For $\mathbf{x}$ at $\partial\mathbb{D}_R$ the Green's function $G(\mathbf{x},\mathbf{x}_A,\omega)$ is purely upgoing, since the upper half-space is homogeneous and the virtual source at $\mathbf{x}_A$ lies in the lower half-space. Similarly, $G^*(\mathbf{x},\mathbf{x}_A,\omega)$ is downgoing at $\partial\mathbb{D}_R$, except for the evanescent field (which we already neglected at $\partial\mathbb{D}_R$ in the derivation of equation (11)). Hence, we may write

$$p^-(\mathbf{x},\omega) \quad = \quad G(\mathbf{x},\mathbf{x}_A,\omega), \quad \text{for} \quad x_3 = x_{3,R}, \tag{34}$$

$$p^+(\mathbf{x},\omega) \quad = \quad G^*(\mathbf{x},\mathbf{x}_A,\omega), \quad \text{for} \quad x_3 = x_{3,R}. \tag{35}$$

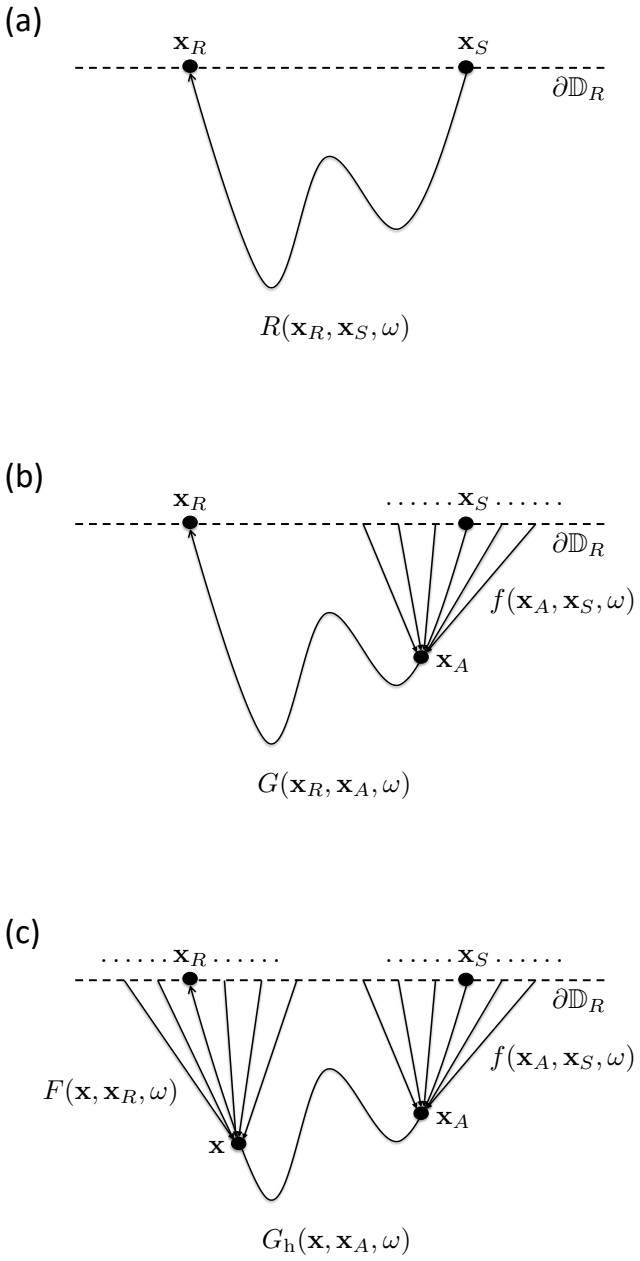

Figure 2. Illustration of source and receiver redatuming as a two-step process. Starting with (a) the reflection response $R(\mathbf{x}_R, \mathbf{x}_S, \omega)$ at the surface, in step one (b) the Green's function $G(\mathbf{x}_R, \mathbf{x}_A, \omega)$ is obtained for a virtual source at $\mathbf{x}_A$, and step two (c) yields the homogeneous Green's function $G_{\rm h}(\mathbf{x}, \mathbf{x}_A, \omega)$ for a virtual receiver at $\mathbf{x}$. All functions in this figure are represented by simple rays, but in reality these are wave fields, including primaries, multiples, refracted and evanescent waves.

Substitution of equations (33) − (35) into equation (11) yields

$$G_{\rm h}(\mathbf{x}, \mathbf{x}_A, \omega) = \int_{\partial\mathbb{D}_R} F(\mathbf{x}, \mathbf{x}_R, \omega) G(\mathbf{x}_R, \mathbf{x}_A, \omega) {\rm d}\mathbf{x}_R + \int_{\partial\mathbb{D}_R} F^*(\mathbf{x}, \mathbf{x}_R, \omega) G^*(\mathbf{x}_R, \mathbf{x}_A, \omega) {\rm d}\mathbf{x}_R, \quad \text{for} \quad x_3 \geq x_{3,R}, \tag{36}$$

or

$$G_{\rm h}(\mathbf{x},\mathbf{x}_A,\omega) \quad = \quad 2\Re\int_{\partial\mathbb{D}_R} F(\mathbf{x},\mathbf{x}_R,\omega)G(\mathbf{x}_R,\mathbf{x}_A,\omega){\rm d}\mathbf{x}_R, \quad \text{for} \quad x_3 \geq x_{3,R}, \tag{37}$$

where $\Re$ denotes that the real part is taken. This equation describes redatuming of the receivers from all $\mathbf{x}_R$ at the surface to virtual-receiver position $\mathbf{x}$ in the subsurface, see Figure 2(c). It gives the homogeneous Green's function $G_{\rm h}(\mathbf{x},\mathbf{x}_A,\omega)$, which is the response to the virtual source at $\mathbf{x}_A$, observed by a virtual receiver at $\mathbf{x}$, plus its complex conjugate. After transforming this to the time domain we obtain

$$G_{\rm h}(\mathbf{x},\mathbf{x}_A,t) = G(\mathbf{x},\mathbf{x}_A,t) + G(\mathbf{x},\mathbf{x}_A,-t). \tag{38}$$

The two functions at the right-hand side do not overlap in time (except for $\mathbf{x} = \mathbf{x}_A$ and only for $t = 0$), hence, $G(\mathbf{x},\mathbf{x}_A,t)$ can be extracted from $G_{\rm h}(\mathbf{x},\mathbf{x}_A,t)$ by selecting its causal part.

Note that there is an unbalance in the focusing functions used for source redatuming ($f(\mathbf{x}_A,\mathbf{x}_S,\omega)$ in equation (30)) and for receiver redatuming ($F(\mathbf{x},\mathbf{x}_R,\omega)$ in equation (37)), see also Figure 2(c). This is due to the difference in types of responses at the surface (the dipole response $R(\mathbf{x}_R,\mathbf{x}_S,\omega)$) and in the subsurface (the monopole response $G_{\rm h}(\mathbf{x},\mathbf{x}_A,\omega)$). When the response at the surface were also a monopole response, then the focusing function $f(\mathbf{x}_A,\mathbf{x}_S,\omega)$ for source redatuming should be replaced by $F(\mathbf{x}_A,\mathbf{x}_S,\omega)$.

Homogeneous Green's function representations similar to equation (37) were also derived by Wapenaar et al. (2016a), Van der Neut et al. (2017) and Singh & Snieder (2017), but here it has been derived without decomposition inside the medium. Hence, it also holds for evanescent waves inside the medium, as long as condition (12) is obeyed. Moreover, the derivation presented here is much simpler than in those references.

The source and receiver redatuming processes can be captured in one equation by substituting equation (30) into (37). This gives

$$\begin{aligned} G_{\rm h}(\mathbf{x},\mathbf{x}_A,\omega) \quad &= \quad 2\Re\int_{\partial\mathbb{D}_R}\int_{\partial\mathbb{D}_R} F(\mathbf{x},\mathbf{x}_R,\omega)R(\mathbf{x}_R,\mathbf{x}_S,\omega)f(\mathbf{x}_A,\mathbf{x}_S,\omega){\rm d}\mathbf{x}_S{\rm d}\mathbf{x}_R \\ &+ \quad 2\Re\int_{\partial\mathbb{D}_R} F(\mathbf{x},\mathbf{x}_R,\omega)f^*(\mathbf{x}_A,\mathbf{x}_R,\omega){\rm d}\mathbf{x}_R, \quad \text{for} \quad \{x_3,x_{3,A}\} \geq x_{3,R}. \end{aligned} \tag{39}$$

The double integral on the right-hand side resembles the process of classical source and receiver redatuming (Berkhout, 1982; Berryhill, 1984), but with the primary focusing functions in those references replaced by full-field focusing functions. It also resembles source-receiver interferometry (Curtis & Halliday, 2010), but with the double integration along a closed boundary in that paper replaced by the double integration over the open boundary $\partial\mathbb{D}_R$. Hence, via the theories of primary source-receiver redatuming (Berkhout, 1982; Berryhill, 1984), closed-boundary source-receiver interferometry (Curtis & Halliday, 2010) and open-boundary homogeneous Green's function retrieval of decomposed wave fields (Wapenaar et al., 2016a; Van der Neut et al., 2017; Singh & Snieder, 2017), we have arrived at a representation for open-boundary homogeneous Green's function retrieval of full wave fields (equation 39), which accounts for internal multiples, refracted and evanescent waves in the lower half-space. In section 5.3 this representation is extended for the elastodynamic situation.

3.4 Numerical examples

We illustrate the representations of sections 3.2 and 3.3 with numerical examples. Our main aim is to show that these representations hold for evanescent waves inside the medium. To this end we consider oblique plane waves in a horizontally layered medium, with isotropic depth-dependent medium parameters $c(x_3)$ (propagation velocity) and $\rho(x_3)$ (mass density). We consider a horizontally layered medium because in this case we can unequivocally distinguish between propagating and evanescent waves. However, as discussed in section 2, the representations also account for evanescent waves in more general inhomogeneous media. We define the spatial Fourier transform of a space- and frequency-dependent function $u(\mathbf{x},\omega)$ as

$$\tilde{u}(\mathbf{s},x_3,\omega) = \int_{\mathbb{R}^2} \exp\{-i\omega\mathbf{s}\cdot\mathbf{x}_{\rm H}\}u(\mathbf{x}_{\rm H},x_3,\omega){\rm d}\mathbf{x}_{\rm H}, \tag{40}$$

with $\mathbf{s} = (s_1,s_2)$, where s_1 and s_2 are horizontal slownesses and $\mathbb{R}$ is the set of real numbers. This decomposes the function $u(\mathbf{x},\omega)$ into monochromatic plane-wave components. Next, we define the inverse temporal Fourier transform

per slowness value as

$$u(\mathbf{s}, x_3, \tau) = \frac{1}{\pi}\Re \int_0^\infty \tilde{u}(\mathbf{s}, x_3, \omega) \exp\{-i\omega\tau)\mathrm{d}\omega, \tag{41}$$

where τ is the so-called intercept time (Stoffa, 1989).

First we investigate the representation of equation (24) and take $\mathbf{x}_S = (0, 0, x_{3,R})$. We use the definitions of equations (40) and (41) to transform this representation to the slowness intercept-time domain. Taking into account that for a horizontally layered, isotropic medium all functions in equation (24) are cylindrically symmetric, it suffices to consider the transformed representation for one slowness variable only. We thus obtain

$$\begin{aligned} G(s_1, x_3, x_{3,R}, \tau) &= \int_{-\infty}^{\tau} f(s_1, x_3, x_{3,R}, \tau')R(s_1, x_{3,R}, \tau - \tau')\mathrm{d}\tau' \\ &+ f(s_1, x_3, x_{3,R}, -\tau), \quad \text{for} \quad x_3 \geq x_{3,R}. \end{aligned} \tag{42}$$

For any given value of s_1, the Green's function $G(s_1, x_3, x_{3,R}, \tau)$ is the response to a plane-wave source at $x_{3,R}$ as a function of receiver depth x_3 and intercept time τ. For $|s_1| \leq 1/c(x_3)$ the plane wave is propagating, whereas for $|s_1| > 1/c(x_3)$ it is evanescent. For propagating waves, the local propagation angle $\alpha(x_3)$ follows from $s_1 = \sin\alpha(x_3)/c(x_3)$. The focusing function $f(s_1, x_3, x_{3,R}, \tau)$ obeys the focusing condition formulated by equation (25), transformed to the slowness intercept-time domain, hence

$$f(s_1, x_3, x_{3,R}, \tau)|_{x_3 = x_{3,R}} = \frac{\rho_0 c_0}{2\cos\alpha_0}\delta(\tau), \tag{43}$$

with $\alpha_0 = \alpha(x_{3,R})$. Consider the horizontally layered medium of Figure 3(a). Two thin high-velocity layers ($c_2 = c_4 =$ 3000 m/s) are embedded in a homogeneous background medium with a velocity of 2000 m/s. The mass densities, in kg m^{-3}, are assigned the same numerical values as the velocities to get significant contrasts between the different layers. A plane wave is emitted from $x_{3,R}$ into the medium, with slowness $s_1 = 1/2800$ s m^{-1}, hence, this wave leaves the surface with an angle $\alpha_0 = 45.6^o$ and becomes evanescent in the high-velocity layers. For the source function we use a Ricker wavelet with a central frequency of 50 Hz, hence, the wavelength for the central frequency in the high-velocity layers is 60 m. The thickness of the high-velocity layers is 20 m, which is small compared with the wavelength, hence, we may expect that the waves tunnel through these layers. Figure 3(b) shows the numerically modelled reflection response $R(s_1, x_{3,R}, \tau)$ for the chosen slowness. The first two events are composite reflections from the two high-velocity layers (including internal multiples of evanescent waves inside these layers) and the other events are multiple reflections between these layers. Figure 3(c) shows the numerically modelled focusing function $f(s_1, x_3, x_{3,R}, \tau)$ as a function of x_3 and τ, convolved with the same Ricker wavelet for a clear display. Blue and red arrows indicate upgoing and downgoing waves, respectively, in the homogeneous background medium. The tunnelling of the waves through the high-velocity layers is clearly visible. A single upgoing wave reaches the surface $x_{3,R}$ at $\tau = 0$, conform the focusing condition formulated by equation (43) (except that in this display $\delta(\tau)$ is convolved with the Ricker wavelet). Note that the amplitude increases with increasing depth (to compensate for the evanescent waves in the high-velocity layers), which means that, in practice, the numerically computed focusing function becomes unstable beyond some depth.

The reflection response of Figure 3(b) and the focusing function of Figure 3(c) (the latter without the wavelet) are used as input for the representation of equation (42). This yields the Green's function $G(s_1, x_3, x_{3,R}, \tau)$ (convolved with the Ricker wavelet) as a function of x_3 and τ, see Figure 4(a). Blue and red arrows indicate again upgoing and downgoing waves, respectively. This figure shows the expected behaviour of the response to a plane-wave source at $x_{3,R}$ (a downgoing wave leaving the surface, two composite primary upgoing waves and multiple reflections between the high velocity layers). Figure 4(b) shows $G(s_1, x_{3,A}, x_{3,R}, \tau)$ for $x_{3,A} = 300$ m. The green line is the Green's function obtained from equation (42), the red line is the directly modelled Green's function. Similarly, Figure 4(c) shows $G(s_1, x_{3,B}, x_{3,R}, \tau)$ for $x_{3,B} = 210$ m, i.e., inside the first high velocity layer. In both cases the match is perfect, which confirms that the representation of equation (42) correctly accounts for propagating and evanescent waves inside the medium.

Using source-receiver reciprocity we may interpret Figure 4(b) as $G(s_1, x_{3,R}, x_{3,A}, \tau)$, which is the response at the surface $x_{3,R}$ to a virtual plane-wave source at $x_{3,A} = 300$ m. Hence, $G(s_1, x_{3,R}, x_{3,A}, \tau)$ may be seen as the result of redatuming the source from the surface to $x_{3,A}$. We now discuss receiver redatuming. To this end, we transform

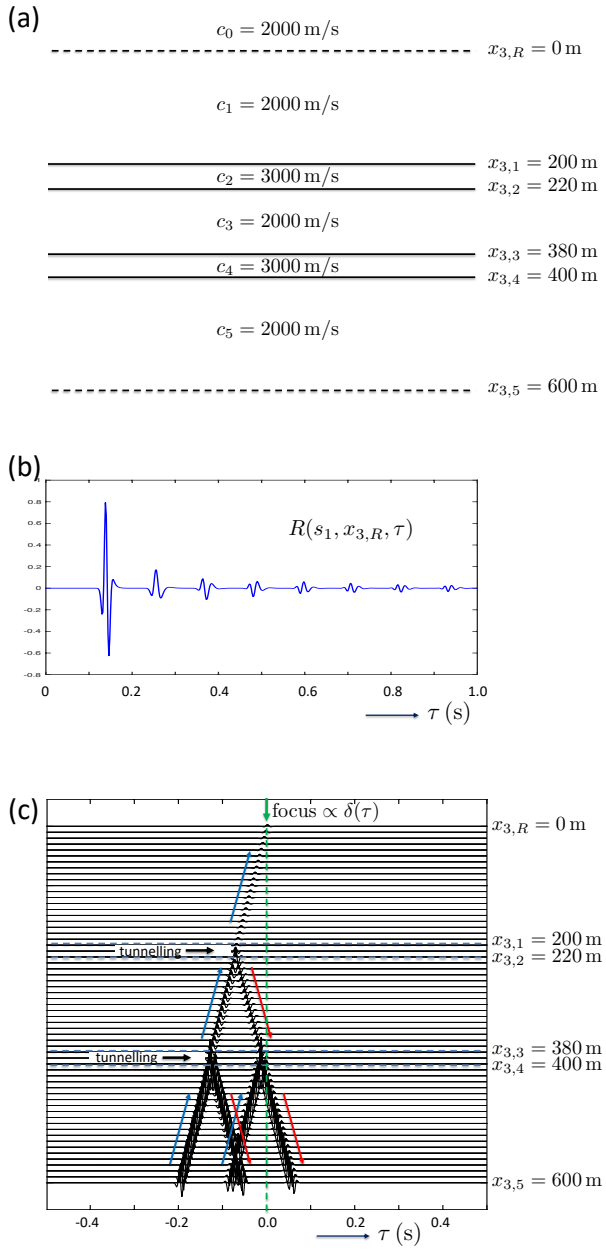

Figure 3. (a) Horizontally layered medium with two high-velocity layers. (b) Numerically modelled reflection response $R(s_1, x_{3,R}, \tau)$ at the surface. The horizontal slowness $s_1 = 1/2800$ s m^{-1} is chosen such that the wave field is evanescent in the high-velocity layers. (c) Numerically modelled focusing function $f(s_1, x_3, x_{3,R}, \tau)$. The trace at $x_{3,R} = 0$ m illustrates the focusing condition of equation (43).

the representation of equation (36) to the slowness intercept-time domain, which yields

$$\begin{aligned} G_{\mathrm{h}}(s_1, x_3, x_{3,A}, \tau) &= \int_{-\infty}^{\tau} F(s_1, x_3, x_{3,R}, \tau') G(s_1, x_{3,R}, x_{3,A}, \tau - \tau') \mathrm{d}\tau' \\ &+ \int_{\tau}^{\infty} F(s_1, x_3, x_{3,R}, -\tau') G(s_1, x_{3,R}, x_{3,A}, \tau' - \tau) \mathrm{d}\tau', \\ &\qquad \text{for} \quad x_3 \geq x_{3,R}, \end{aligned} \tag{44}$$

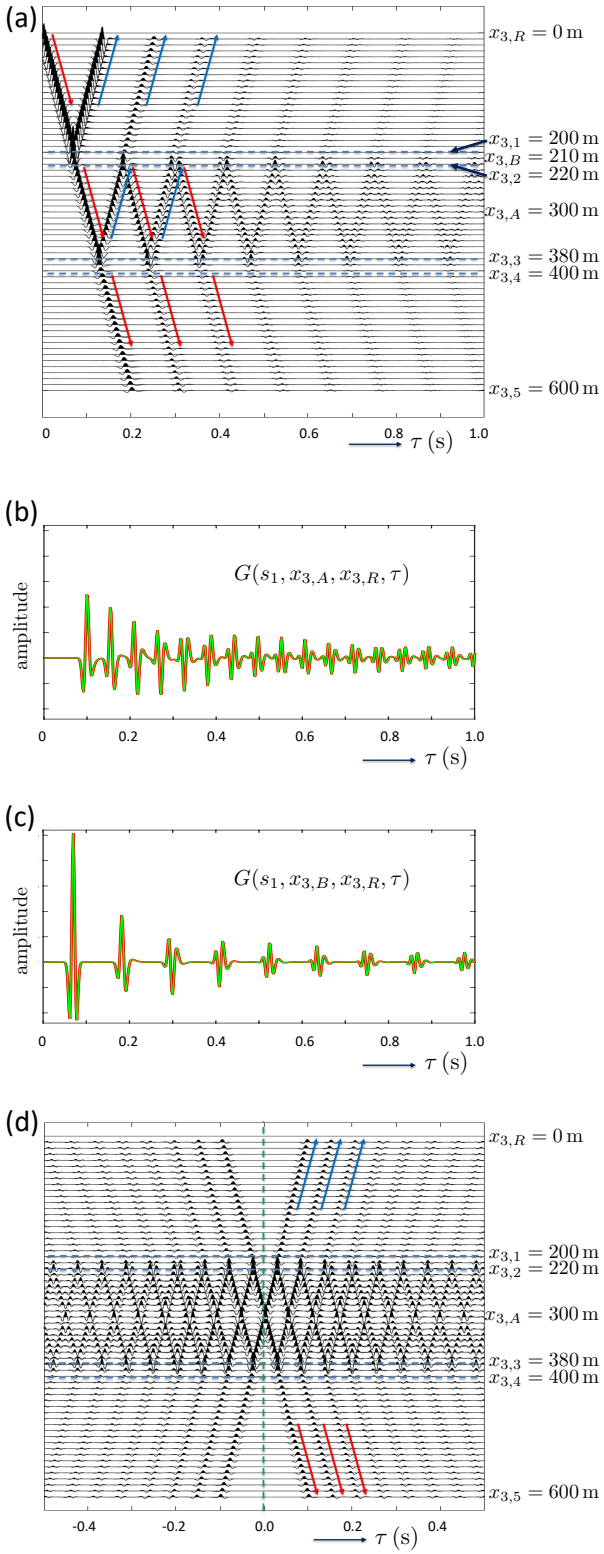

Figure 4. (a) Green's function $G(s_1, x_3, x_{3,R}, \tau)$ obtained from Figures 3(b) and 3(c) via the representation of equation (42). (b) $G(s_1, x_{3,A}, x_{3,R}, \tau)$, taken from figure (a) for $x_{3,A} = 300$ m (green), compared with directly modelled Green's function (red). (c) Similarly, $G(s_1, x_{3,B}, x_{3,R}, \tau)$, taken from figure (a) for $x_{3,B} = 210$ m inside the first high velocity layer. (d) Homogeneous Green's function $G_{\rm h}(s_1, x_3, x_{3,A}, \tau)$ obtained from Figures 3(c) and 4(b) via the representation of equation (44).

with, analogous to equation (19),

$$F(s_1, x_3, x_{3,R}, \tau) = \frac{2\cos\alpha_0}{\rho_0 c_0} f(s_1, x_3, x_{3,R}, \tau). \tag{45}$$

Note that the right-hand side of equation (44) contains the Green's function with the redatumed source at $x_{3,A}$ and the receiver at the surface. This representation redatums the receiver from $x_{3,R}$ to any depth x_3 in the subsurface. This yields the homogeneous Green's function, which consists of $G(s_1, x_3, x_{3,A}, \tau)$ plus its time-reversal, see Figure 4(d). The causal part (right of the green dashed line) is the retrieved Green's function $G(s_1, x_3, x_{3,A}, \tau)$. Conform expectation, we see a virtual source at $x_{3,A}$ emitting downgoing and upgoing plane waves, which reverberate in the wave guide between the two high-velocity layers, but which also emit some energy through tunneling into the half-spaces above and below the high-velocity layers. This example illustrates the handling of propagating and evanescent waves inside the medium by the homogeneous Green's function representation of equation (44).

4 ELASTODYNAMIC WAVE FIELD REPRESENTATION

We derive the elastodynamic equivalent of the representation of equation (11). We consider the same configuration as in section 2, except that now the medium parameters of the lower half-space $x_3 > x_{3,R}$ are the stiffness tensor $c_{ijkl}(\mathbf{x})$ and the mass density tensor $\rho_{ik}(\mathbf{x})$, with symmetries $c_{ijkl} = c_{jikl} = c_{ijlk} = c_{klij}$ and $\rho_{ik} = \rho_{ki}$. In the homogeneous isotropic upper half-space $x_3 \leq x_{3,R}$ the parameters are $\rho_{ik} = \delta_{ik}\rho_0$ and $c_{ijkl} = \lambda_0\delta_{ij}\delta_{kl} + \mu_0(\delta_{ik}\delta_{jl} + \delta_{il}\delta_{jk})$, with λ_0 and μ_0 the Lamé parameters of the half-space. The P- and S-wave propagation velocities of the upper half-space are $c_P = ((\lambda_0 + 2\mu_0)/\rho_0)^{1/2}$ and $c_S = (\mu_0/\rho_0)^{1/2}$, respectively.

The basic equations in the frequency domain for elastodynamic wave propagation are the linearized equation of motion

$$-i\omega\rho_{ik}v_k - \partial_j\tau_{ij} \quad = \quad \hat{f}_i \tag{46}$$

and the linearized deformation equation

$$i\omega\tau_{ij} + c_{ijkl}\partial_l v_k \quad = \quad 0, \tag{47}$$

respectively. Here $\tau_{ij}(\mathbf{x}, \omega)$ is the stress tensor (with symmetry $\tau_{ij} = \tau_{ji}$), $v_k(\mathbf{x}, \omega)$ the particle velocity and $\hat{f}_i(\mathbf{x}, \omega)$ a source in terms of volume-force density (the circumflex is used to distinguish this source term from the focusing function). Equations (46) and (47) can be combined into the elastodynamic wave equation

$$L_{ik}v_k = i\omega\hat{f}_i, \tag{48}$$

with

$$L_{ik} = \partial_j c_{ijkl}\partial_l + \omega^2\rho_{ik}. \tag{49}$$

We introduce a focusing function $\mathbf{F}(\mathbf{x}, \mathbf{x}_R, \omega)$ as a 3×3 matrix, according to

$$\mathbf{F}(\mathbf{x}, \mathbf{x}_R, \omega) = \begin{pmatrix} F_{1,1} & F_{1,2} & F_{1,3} \\ F_{2,1} & F_{2,2} & F_{2,3} \\ F_{3,1} & F_{3,2} & F_{3,3} \end{pmatrix} (\mathbf{x}, \mathbf{x}_R, \omega), \tag{50}$$

where $\mathbf{x}_R$ denotes again the position of a focal point at $\partial\mathbb{D}_R$. Each column of $\mathbf{F}$ is a particle velocity vector of which the components, for fixed $\mathbf{x}_R$ and variable $\mathbf{x}$, obey the elastodynamic wave equation (48) for the source-free situation. We define the focusing property, analogous to equation (9), as

$$\mathbf{F}(\mathbf{x}, \mathbf{x}_R, \omega)|_{x_3 = x_{3,R}} \quad = \quad \mathbf{I}\delta(\mathbf{x}_\mathrm{H} - \mathbf{x}_{\mathrm{H},R}), \tag{51}$$

($\mathbf{I}$ is the 3×3 identity matrix) and demand that $\mathbf{F}(\mathbf{x}, \mathbf{x}_R, \omega)$ is purely upgoing at $\partial\mathbb{D}_R$ and in the homogeneous isotropic upper half-space.

We discuss a representation for a wave field $v_k(\mathbf{x}, \omega)$, which may have sources in the upper half-space above $\partial\mathbb{D}_R$, but which obeys the source-free wave equation $L_{ik}v_k = 0$ for $x_3 \geq x_{3,R}$. We store the components $v_k(\mathbf{x}, \omega)$ in a 3×1

vector $\mathbf{v}(\mathbf{x},\omega)$ as follows

$$\mathbf{v}(\mathbf{x},\omega) = \begin{pmatrix} v_1 \\ v_2 \\ v_3 \end{pmatrix} (\mathbf{x},\omega). \tag{52}$$

In the lower half-space we express $\mathbf{v}(\mathbf{x},\omega)$ as a superposition of mutually independent wave fields that obey the same source-free wave equation for $x_3 \geq x_{3,R}$. For this purpose we choose the focusing functions $\mathbf{F}(\mathbf{x},\mathbf{x}_R,\omega)$ and $\mathbf{F}^*(\mathbf{x},\mathbf{x}_R,\omega)$, of which the columns are also mutually independent. Hence, analogous to equation (10) we express $\mathbf{v}(\mathbf{x},\omega)$ as

$$\mathbf{v}(\mathbf{x},\omega) = \int_{\partial\mathbb{D}_R} \mathbf{F}(\mathbf{x},\mathbf{x}_R,\omega)\mathbf{a}(\mathbf{x}_R,\omega)\mathrm{d}\mathbf{x}_R + \int_{\partial\mathbb{D}_R} \mathbf{F}^*(\mathbf{x},\mathbf{x}_R,\omega)\mathbf{b}(\mathbf{x}_R,\omega)\mathrm{d}\mathbf{x}_R, \quad \text{for} \quad x_3 \geq x_{3,R}. \tag{53}$$

Here $\mathbf{a}(\mathbf{x}_R,\omega)$ and $\mathbf{b}(\mathbf{x}_R,\omega)$ are yet undetermined 3×1 vectors. In Appendix B1 we formulate two boundary conditions at $\partial\mathbb{D}_R$, from which we solve $\mathbf{a}(\mathbf{x}_R,\omega)$ and $\mathbf{b}(\mathbf{x}_R,\omega)$. We thus obtain

$$\mathbf{v}(\mathbf{x},\omega) = \int_{\partial\mathbb{D}_R} \mathbf{F}(\mathbf{x},\mathbf{x}_R,\omega)\mathbf{v}^-(\mathbf{x}_R,\omega)\mathrm{d}\mathbf{x}_R + \int_{\partial\mathbb{D}_R} \mathbf{F}^*(\mathbf{x},\mathbf{x}_R,\omega)\mathbf{v}^+(\mathbf{x}_R,\omega)\mathrm{d}\mathbf{x}_R, \quad \text{for} \quad x_3 \geq x_{3,R}, \tag{54}$$

where $\mathbf{v}^-(\mathbf{x}_R,\omega)$ and $\mathbf{v}^+(\mathbf{x}_R,\omega)$ represent the upgoing and downgoing parts, respectively, of $\mathbf{v}(\mathbf{x}_R,\omega)$ for $\mathbf{x}_R$ at $\partial\mathbb{D}_R$. As for the acoustic representation of equation (11), the underlying assumption in the derivation of equation (54) is that evanescent waves can be neglected at $\partial\mathbb{D}_R$. Hence, it only holds for waves which have a horizontal slowness $\mathbf{s}$ which obeys

$$|\mathbf{s}| \leq 1/c_P, \quad \text{at } \partial\mathbb{D}_R. \tag{55}$$

Using similar arguments as given below equation (12), it follows that equation (54) accounts for evanescent waves inside the medium, as long as they are related to propagating waves at the surface, as formulated by equation (55).

5 ELASTODYNAMIC GREEN'S FUNCTION REPRESENTATIONS

5.1 Representation for a modified elastodynamic Green's function

We introduce the elastodynamic Green's function $G_{k,n}(\mathbf{x},\mathbf{x}_S,\omega)$ as a solution of equation (48) for a unit point source of volume-force density at $\mathbf{x}_S$ in the x_n-direction, hence

$$L_{ik}G_{k,n} = i\omega\delta_{in}\delta(\mathbf{x}-\mathbf{x}_S). \tag{56}$$

We demand that the time domain version of $G_{k,n}(\mathbf{x},\mathbf{x}_S,\omega)$ is causal. Note that $G_{k,n}$ obeys source-receiver reciprocity, i.e., $G_{k,n}(\mathbf{x},\mathbf{x}_S,\omega) = G_{n,k}(\mathbf{x}_S,\mathbf{x},\omega)$. We introduce $\mathbf{G}(\mathbf{x},\mathbf{x}_S,\omega)$ as a 3×3 matrix, according to

$$\mathbf{G}(\mathbf{x},\mathbf{x}_S,\omega) = \begin{pmatrix} G_{1,1} & G_{1,2} & G_{1,3} \\ G_{2,1} & G_{2,2} & G_{2,3} \\ G_{3,1} & G_{3,2} & G_{3,3} \end{pmatrix} (\mathbf{x},\mathbf{x}_S,\omega). \tag{57}$$

Each column is a particle velocity vector of which the components, for fixed $\mathbf{x}_S$ and variable $\mathbf{x}$, obey wave equation (56). The different columns correspond to different directions of the force source at $\mathbf{x}_S$. In matrix form, source-receiver reciprocity implies $\mathbf{G}(\mathbf{x},\mathbf{x}_S,\omega) = \{\mathbf{G}(\mathbf{x}_S,\mathbf{x},\omega)\}^t$, where superscript t denotes transposition.

We choose $\mathbf{x}_S = (\mathbf{x}_{\mathrm{H},S}, x_{3,S})$ again in the upper half-space, at a vanishing distance ϵ above $\partial\mathbb{D}_R$, hence, $x_{3,S} = x_{3,R} - \epsilon$. In Appendix B2 we derive a modified version $\mathbf{\Gamma}(\mathbf{x},\mathbf{x}_S,\omega)$ of $\mathbf{G}(\mathbf{x},\mathbf{x}_S,\omega)$ (equation B19), of which the downgoing part $\mathbf{\Gamma}^+(\mathbf{x},\mathbf{x}_S,\omega)$ for $\mathbf{x}$ at $\partial\mathbb{D}_R$ (i.e., just below the source) is equal to a spatial delta function. Hence

$$\mathbf{\Gamma}^+(\mathbf{x},\mathbf{x}_S,\omega)|_{x_3=x_{3,R}} = \mathbf{I}\delta(\mathbf{x}_\mathrm{H}-\mathbf{x}_{\mathrm{H},S}). \tag{58}$$

We define the reflection response $\mathbf{R}(\mathbf{x}_R,\mathbf{x}_S,\omega)$ of the medium below $\partial\mathbb{D}_R$ as the upgoing part of $\mathbf{\Gamma}(\mathbf{x}_R,\mathbf{x}_S,\omega)$, with

$\mathbf{x}_R$ at $\partial\mathbb{D}_R$, hence

$$\mathbf{R}(\mathbf{x}_R,\mathbf{x}_S,\omega) \quad = \quad \mathbf{\Gamma}^{-}(\mathbf{x}_R,\mathbf{x}_S,\omega). \tag{59}$$

Substituting $\mathbf{v}(\mathbf{x},\omega)=\mathbf{\Gamma}(\mathbf{x},\mathbf{x}_S,\omega)$ and $\mathbf{v}^{\pm}(\mathbf{x}_R,\omega)=\mathbf{\Gamma}^{\pm}(\mathbf{x}_R,\mathbf{x}_S,\omega)$ into equation (54), using equations (58) and (59), gives

$$\mathbf{\Gamma}(\mathbf{x},\mathbf{x}_S,\omega) \quad = \quad \int_{\partial\mathbb{D}_R}\mathbf{F}(\mathbf{x},\mathbf{x}_R,\omega)\mathbf{R}(\mathbf{x}_R,\mathbf{x}_S,\omega)\mathrm{d}\mathbf{x}_R+\mathbf{F}^{*}(\mathbf{x},\mathbf{x}_S,\omega), \quad \text{for} \quad x_3\geq x_{3,R}. \tag{60}$$

This is a representation for the modified version $\mathbf{\Gamma}(\mathbf{x},\mathbf{x}_S,\omega)$ of the elastodynamic Green's function. It has been derived without applying decomposition in the lower half-space. It excludes the contribution from waves that are evanescent at $\partial\mathbb{D}_R$.

5.2 Representation for the elastodynamic Green's function

In Appendix B3 we show that equation (60) can be reorganized into the following representation for the elastodynamic Green's function $\mathbf{G}(\mathbf{x},\mathbf{x}_S,\omega)$

$$\mathbf{G}(\mathbf{x},\mathbf{x}_S,\omega) \quad = \quad \int_{\partial\mathbb{D}_R}\mathbf{f}(\mathbf{x},\mathbf{x}_R,\omega)\{\mathbf{R}(\mathbf{x}_S,\mathbf{x}_R,\omega)\}^{t}\mathrm{d}\mathbf{x}_R+\mathbf{f}^{*}(\mathbf{x},\mathbf{x}_S,\omega), \quad \text{for} \quad x_3\geq x_{3,R}. \tag{61}$$

Here $\mathbf{f}(\mathbf{x},\mathbf{x}_R,\omega)$ is a modified version of the focusing function $\mathbf{F}(\mathbf{x},\mathbf{x}_R,\omega)$ (equation B24). This representation gives the full elastodynamic particle velocity field at any virtual receiver position $\mathbf{x}$ inside the medium. It is similar to earlier derived elastodynamic representations for the Marchenko method (Wapenaar & Slob, 2014; da Costa Filho et al., 2014), but here it has been derived without applying decomposition at a truncation level inside the medium. As a consequence, equation (61) gives the full wave field at any virtual receiver position $\mathbf{x}$ inside the medium, including multiply reflected, converted, refracted and evanescent waves. This representation only excludes the contribution from waves that are evanescent at $\partial\mathbb{D}_R$, see the condition formulated by equation (55). Applying elastodynamic representations like the one in equation (61) to derive a Marchenko method is not trivial. The functions $\mathbf{G}(\mathbf{x},\mathbf{x}_S,\omega)$ and $\mathbf{f}^{*}(\mathbf{x},\mathbf{x}_S,\omega)$, transformed back to the time domain, partly overlap and hence they cannot be completely separated by a time window (Wapenaar & Slob, 2014; Reinicke et al., 2020). A discussion of elastodynamic Marchenko methods is beyond the scope of this paper.

Similar as in the acoustic situation, the representation of equation (61) is not a sufficient starting point for imaging. We need at least one other type of field at $\mathbf{x}$, next to $\mathbf{G}(\mathbf{x},\mathbf{x}_S,\omega)$, which represents the particle velocity at $\mathbf{x}$ in response to force sources at $\mathbf{x}_S$. To this end, we introduce a Green's function $\mathbf{G}^{\tau}_j(\mathbf{x},\mathbf{x}_S,\omega)$ which, for $j=1,2,3$, stands for the three traction vectors at $\mathbf{x}$. From equation (47) we derive that the traction vector $\boldsymbol{\tau}_j$ can be expressed in terms of the particle velocity as $\boldsymbol{\tau}_j=-\frac{1}{i\omega}\mathbf{C}_{jl}\partial_l\mathbf{v}$, with $(\boldsymbol{\tau}_j)_i=\tau_{ij}$ and $(\mathbf{C}_{jl})_{ik}=c_{ijkl}$. Similarly, we relate $\mathbf{G}^{\tau}_j$ to $\mathbf{G}$ via

$$\mathbf{G}^{\tau}_j(\mathbf{x},\mathbf{x}_S,\omega)=-\frac{1}{i\omega}\mathbf{C}_{jl}(\mathbf{x})\partial_l\mathbf{G}(\mathbf{x},\mathbf{x}_S,\omega). \tag{62}$$

Hence, when $\mathbf{G}(\mathbf{x},\mathbf{x}_S,\omega)$ is available on a sufficiently dense grid, $\mathbf{G}^{\tau}_j(\mathbf{x},\mathbf{x}_S,\omega)$ can be obtained via equation (62). Alternatively, $\mathbf{G}^{\tau}_j(\mathbf{x},\mathbf{x}_S,\omega)$ can be obtained from a modified version of the representation for $\mathbf{G}(\mathbf{x},\mathbf{x}_S,\omega)$. Applying the operation $-\frac{1}{i\omega}\mathbf{C}_{jl}\partial_l$ to both sides of equation (61) yields

$$\mathbf{G}^{\tau}_j(\mathbf{x},\mathbf{x}_S,\omega) \quad = \quad \int_{\partial\mathbb{D}_R}\mathbf{h}_j(\mathbf{x},\mathbf{x}_R,\omega)\{\mathbf{R}(\mathbf{x}_S,\mathbf{x}_R,\omega)\}^{t}\mathrm{d}\mathbf{x}_R-\mathbf{h}^{*}_j(\mathbf{x},\mathbf{x}_S,\omega), \text{ for } \quad x_3\geq x_{3,R}, \tag{63}$$

with

$$\mathbf{h}_j(\mathbf{x},\mathbf{x}_R,\omega)=-\frac{1}{i\omega}\mathbf{C}_{jl}(\mathbf{x})\partial_l\mathbf{f}(\mathbf{x},\mathbf{x}_R,\omega). \tag{64}$$

The Green's functions $\mathbf{G}(\mathbf{x},\mathbf{x}_S,\omega)$ and $\mathbf{G}^{\tau}_j(\mathbf{x},\mathbf{x}_S,\omega)$ together provide sufficient information for imaging.

5.3 Representation for the homogeneous elastodynamic Green's function

The representations in sections 5.1 and 5.2 give the elastodynamic response to a source at $\mathbf{x}_S$, observed by a virtual receiver at $\mathbf{x}$ inside the medium. Similar as in section 3.3, here we modify this representation, to create the response

at the surface to a virtual source inside the medium. After that, we show how to obtain the response to this virtual source at a virtual receiver inside the medium.

We start by renaming the coordinate vectors in equation (61) as follows: $\mathbf{x}_S \rightarrow \mathbf{x}_R$, $\mathbf{x}_R \rightarrow \mathbf{x}_S$, $\mathbf{x} \rightarrow \mathbf{x}_A$. This yields, in combination with transposing all terms and applying source-receiver reciprocity on the left-hand side of equation (61),

$$\mathbf{G}(\mathbf{x}_R, \mathbf{x}_A, \omega) \quad = \quad \int_{\partial\mathbb{D}_R} \mathbf{R}(\mathbf{x}_R, \mathbf{x}_S, \omega)\mathbf{f}^t(\mathbf{x}_A, \mathbf{x}_S, \omega)\mathrm{d}\mathbf{x}_S + \mathbf{f}^\dagger(\mathbf{x}_A, \mathbf{x}_R, \omega), \text{ for } \quad x_{3,A} \geq x_{3,R}. \tag{65}$$

Here superscript † denotes transposition and complex conjugation. The integral in equation (65) describes elastodynamic redatuming of the sources from all $\mathbf{x}_S$ at the surface to virtual-source position $\mathbf{x}_A$ in the subsurface.

Our next aim is to derive a representation for the response observed by a virtual receiver at $\mathbf{x}$ in the subsurface, given $\mathbf{G}(\mathbf{x}_R, \mathbf{x}_A, \omega)$. Similar as in section 3.3, we define the homogeneous elastodynamic Green's function

$$\mathbf{G}_\mathrm{h}(\mathbf{x}, \mathbf{x}_A, \omega) = \mathbf{G}(\mathbf{x}, \mathbf{x}_A, \omega) + \mathbf{G}^*(\mathbf{x}, \mathbf{x}_A, \omega). \tag{66}$$

The components of the columns in $\mathbf{G}(\mathbf{x}, \mathbf{x}_A, \omega)$ and $\mathbf{G}^*(\mathbf{x}, \mathbf{x}_A, \omega)$ obey equation (56), with source terms $i\omega\delta_{in}\delta(\mathbf{x}-\mathbf{x}_A)$ and $-i\omega\delta_{in}\delta(\mathbf{x}-\mathbf{x}_A)$, respectively, on the right-hand sides. Hence, the components of the columns of $\mathbf{G}_\mathrm{h}(\mathbf{x}, \mathbf{x}_A, \omega)$ obey this equation without a source on the right-hand side. Following a similar reasoning as in section 3.3, we substitute

$$\mathbf{v}(\mathbf{x}, \omega) \quad = \quad \mathbf{G}_\mathrm{h}(\mathbf{x}, \mathbf{x}_A, \omega), \tag{67}$$

$$\mathbf{v}^-(\mathbf{x}, \omega) \quad = \quad \mathbf{G}(\mathbf{x}, \mathbf{x}_A, \omega), \quad \text{for} \quad x_3 = x_{3,R}, \tag{68}$$

$$\mathbf{v}^+(\mathbf{x}, \omega) \quad = \quad \mathbf{G}^*(\mathbf{x}, \mathbf{x}_A, \omega), \quad \text{for} \quad x_3 = x_{3,R}, \tag{69}$$

into equation (54). This gives

$$\mathbf{G}_\mathrm{h}(\mathbf{x}, \mathbf{x}_A, \omega) \quad = \quad 2\Re \int_{\partial\mathbb{D}_R} \mathbf{F}(\mathbf{x}, \mathbf{x}_R, \omega)\mathbf{G}(\mathbf{x}_R, \mathbf{x}_A, \omega)\mathrm{d}\mathbf{x}_R, \quad \text{for} \quad x_3 \geq x_{3,R}. \tag{70}$$

This equation describes elastodynamic redatuming of the receivers from all $\mathbf{x}_R$ at the surface to virtual-receiver position $\mathbf{x}$ in the subsurface. It gives the homogeneous Green's function $\mathbf{G}_\mathrm{h}(\mathbf{x}, \mathbf{x}_A, \omega)$, which is the response to the virtual source at $\mathbf{x}_A$, observed by a virtual receiver at $\mathbf{x}$, plus its complex conjugate. After transforming this to the time domain, $\mathbf{G}(\mathbf{x}, \mathbf{x}_A, t)$ can be extracted from $\mathbf{G}_\mathrm{h}(\mathbf{x}, \mathbf{x}_A, t)$ by selecting its causal part.

An elastodynamic homogeneous Green's function representation similar to equation (70) was also derived by Wapenaar et al. (2016b) and illustrated with numerical examples by Reinicke & Wapenaar (2019), but here it has been derived without decomposition inside the medium. Hence, it also holds for evanescent waves inside the medium, as long as condition (55) is obeyed. Moreover, the derivation presented here is much simpler than in those references.

The source and receiver redatuming processes can be captured in one equation by substituting equation (65) into (70). This gives

$$\begin{aligned}\mathbf{G}_\mathrm{h}(\mathbf{x}, \mathbf{x}_A, \omega) \quad &= \quad 2\Re \int_{\partial\mathbb{D}_R} \int_{\partial\mathbb{D}_R} \mathbf{F}(\mathbf{x}, \mathbf{x}_R, \omega)\mathbf{R}(\mathbf{x}_R, \mathbf{x}_S, \omega)\mathbf{f}^t(\mathbf{x}_A, \mathbf{x}_S, \omega)\mathrm{d}\mathbf{x}_S\mathrm{d}\mathbf{x}_R \\ &+ \quad 2\Re \int_{\partial\mathbb{D}_R} \mathbf{F}(\mathbf{x}, \mathbf{x}_R, \omega)\mathbf{f}^\dagger(\mathbf{x}_A, \mathbf{x}_R, \omega)\mathrm{d}\mathbf{x}_R, \quad \text{for} \quad \{x_3, x_{3,A}\} \geq x_{3,R}.\end{aligned} \tag{71}$$

The double integral on the right-hand side resembles the process of classical elastodynamic source and receiver redatuming (Wapenaar & Berkhout, 1989; Hokstad, 2000), but with the primary focusing functions in those references replaced by full-field focusing functions. It also resembles elastodynamic source-receiver interferometry (Halliday et al., 2012), but with the double integration along a closed boundary in that paper replaced by the double integration over the open boundary $\partial\mathbb{D}_R$. Hence, via the theories of elastodynamic primary source-receiver redatuming (Wapenaar & Berkhout, 1989; Hokstad, 2000), closed-boundary source-receiver interferometry (Halliday et al., 2012) and open-boundary homogeneous Green's function retrieval of decomposed wave fields (Wapenaar et al., 2016b), we have arrived at a representation for elastodynamic open-boundary homogeneous Green's function retrieval of full wave fields (equation 71), which accounts for internal multiples, converted, refracted and evanescent waves in the lower half-space.

6 CONCLUSIONS

We have derived acoustic and elastodynamic Green's function representations in terms of the reflection response at the surface and focusing functions. These representations have the same form as the representations that we derived earlier as the basis for Marchenko redatuming, imaging, monitoring and multiple elimination. However, unlike in our original derivations, we did not assume that the wave field inside the medium can be decomposed into downgoing and upgoing waves and we did not ignore evanescent waves inside the medium. We only neglected the contribution of waves that are evanescent at the acquisition boundary. We have demonstrated with numerical examples that the representations indeed account for evanescent waves inside the medium. The representations form a starting point for new research on Marchenko methods which circumvent the limitations caused by the assumptions underlying the traditional representations. In these new developments, special care should be taken to account for the overlap in time of the Green's function and the time-reversed focusing function.

ACKNOWLEDGEMENTS

We thank Marcin Dukalski and Mert Sinan Recep Kiraz for their comments, which helped us sharpen the message. This work has received funding from the European Union's Horizon 2020 research and innovation programme: European Research Council (grant agreement 742703).

Data Availability

No data have been used for this study.

APPENDIX A: DERIVATION OF THE ACOUSTIC WAVE FIELD REPRESENTATION

A1 Derivation of the coefficients in equation (10)

We derive expressions for the coefficients $a(\mathbf{x}_R,\omega)$ and $b(\mathbf{x}_R,\omega)$ in the acoustic wave field representation of equation (10). We do this by formulating two boundary conditions at $\partial\mathbb{D}_R$. First, we consider the acoustic pressure $p(\mathbf{x},\omega)$ at $\partial\mathbb{D}_R$. To this end, we evaluate equation (10) for $\mathbf{x}$ at $\partial\mathbb{D}_R$. Using the focusing condition formulated in equation (9) we thus obtain

$$\begin{aligned} p(\mathbf{x},\omega)|_{x_3=x_{3,R}} &= \int_{\partial\mathbb{D}_R}\delta(\mathbf{x}_\mathrm{H}-\mathbf{x}_{\mathrm{H},R})a(\mathbf{x}_R,\omega)\mathrm{d}\mathbf{x}_R+\int_{\partial\mathbb{D}_R}\delta(\mathbf{x}_\mathrm{H}-\mathbf{x}_{\mathrm{H},R})b(\mathbf{x}_R,\omega)\mathrm{d}\mathbf{x}_R,\\ &= \{a(\mathbf{x},\omega)+b(\mathbf{x},\omega)\}_{x_3=x_{3,R}}, \end{aligned} \tag{A1}$$

where we used $\mathbf{x}_R=(\mathbf{x}_{\mathrm{H},R},x_{3,R})$. This is our first equation for the coefficients $a(\mathbf{x}_R,\omega)$ and $b(\mathbf{x}_R,\omega)$.

Next, we consider the vertical component of the particle velocity $v_3(\mathbf{x},\omega)$ at $\partial\mathbb{D}_R$. From the Fourier transform of equation (1), using $\rho_{jk}=\delta_{jk}\rho_0$ at $\partial\mathbb{D}_R$, we obtain $v_3(\mathbf{x},\omega)=\frac{1}{i\omega\rho_0}\partial_3 p(\mathbf{x},\omega)$ for $\mathbf{x}$ at $\partial\mathbb{D}_R$. Substituting equation (10) gives

$$\begin{aligned} v_3(\mathbf{x},\omega) &= \frac{1}{i\omega\rho_0}\int_{\partial\mathbb{D}_R}\partial_3 F(\mathbf{x},\mathbf{x}_R,\omega)a(\mathbf{x}_R,\omega)\mathrm{d}\mathbf{x}_R\\ &+ \frac{1}{i\omega\rho_0}\int_{\partial\mathbb{D}_R}\partial_3 F^*(\mathbf{x},\mathbf{x}_R,\omega)b(\mathbf{x}_R,\omega)\mathrm{d}\mathbf{x}_R, \end{aligned} \tag{A2}$$

for $x_3=x_{3,R}$. Applying the spatial Fourier transformation of equation (40) to both sides of equation (A2) gives

$$\begin{aligned} \tilde{v}_3(\mathbf{s},x_3,\omega) &= \frac{1}{i\omega\rho_0}\int_{\partial\mathbb{D}_R}\partial_3\tilde{F}(\mathbf{s},x_3,\mathbf{x}_R,\omega)a(\mathbf{x}_R,\omega)\mathrm{d}\mathbf{x}_R\\ &+ \frac{1}{i\omega\rho_0}\int_{\partial\mathbb{D}_R}\partial_3\tilde{F}^*(-\mathbf{s},x_3,\mathbf{x}_R,\omega)b(\mathbf{x}_R,\omega)\mathrm{d}\mathbf{x}_R, \end{aligned} \tag{A3}$$

for $x_3=x_{3,R}$. At this depth level the focusing function is an upgoing field (see Figure 1), hence it obeys the following

one-way wave equation

$$\partial_3 \tilde{F}(\mathbf{s}, x_3, \mathbf{x}_R, \omega)|_{x_3=x_{3,R}} = -i\omega s_3 \tilde{F}(\mathbf{s}, x_{3,R}, \mathbf{x}_R, \omega), \tag{A4}$$

with the vertical slowness s_3 defined as

$$s_3 = \begin{cases} \sqrt{1/c_0^2 - \mathbf{s}\cdot\mathbf{s}}, & \text{for } \mathbf{s}\cdot\mathbf{s} \le 1/c_0^2 \\ i\sqrt{\mathbf{s}\cdot\mathbf{s} - 1/c_0^2}, & \text{for } \mathbf{s}\cdot\mathbf{s} > 1/c_0^2. \end{cases} \tag{A5}$$

The two expressions in equation (A5) represent the situation for propagating and evanescent waves, respectively. Applying the spatial Fourier transformation of equation (40) to equation (9) we further have

$$\tilde{F}(\mathbf{s}, x_{3,R}, \mathbf{x}_R, \omega) = \exp\{-i\omega\mathbf{s}\cdot\mathbf{x}_{\mathrm{H},R}\}. \tag{A6}$$

Substitution of equations (A4) and (A6) into equation (A3) for $x_3 = x_{3,R}$ gives

$$\begin{aligned} &\tilde{v}_3(\mathbf{s}, x_{3,R}, \omega) \\ &= -\frac{s_3}{\rho_0}\int_{\partial\mathbb{D}_R} \exp\{-i\omega\mathbf{s}\cdot\mathbf{x}_{\mathrm{H},R}\} a(\mathbf{x}_R,\omega)\mathrm{d}\mathbf{x}_R + \frac{s_3^*}{\rho_0}\int_{\partial\mathbb{D}_R} \exp\{-i\omega\mathbf{s}\cdot\mathbf{x}_{\mathrm{H},R}\} b(\mathbf{x}_R,\omega)\mathrm{d}\mathbf{x}_R \\ &= -\frac{s_3}{\rho_0}\tilde{a}(\mathbf{s}, x_{3,R}, \omega) + \frac{s_3^*}{\rho_0}\tilde{b}(\mathbf{s}, x_{3,R}, \omega). \end{aligned} \tag{A7}$$

Combining the spatial Fourier transform of equation (A1) with equation (A7) gives

$$\begin{pmatrix} \tilde{p} \\ \tilde{v}_3 \end{pmatrix}_{x_3=x_{3,R}} = \begin{pmatrix} 1 & 1 \\ s_3^*/\rho_0 & -s_3/\rho_0 \end{pmatrix} \begin{pmatrix} \tilde{b} \\ \tilde{a} \end{pmatrix}_{x_3=x_{3,R}}. \tag{A8}$$

For $\mathbf{s}\cdot\mathbf{s} \le 1/c_0^2$ at $\partial\mathbb{D}_R$ we have $s_3^* = s_3$, see equation (A5). Hence, for propagating waves, equation (A8) is recognised as the well-known system that composes the total wave fields on the left-hand side from downgoing and upgoing fields on the right-hand side (Corones, 1975; Ursin, 1983; Fishman & McCoy, 1984). Hence

$$\tilde{b}(\mathbf{s}, x_{3,R}, \omega) = \tilde{p}^+(\mathbf{s}, x_{3,R}, \omega), \tag{A9}$$

$$\tilde{a}(\mathbf{s}, x_{3,R}, \omega) = \tilde{p}^-(\mathbf{s}, x_{3,R}, \omega), \tag{A10}$$

for $\mathbf{s}\cdot\mathbf{s} \le 1/c_0^2$ at $\partial\mathbb{D}_R$. Transforming these expressions back to the space domain, using

$$p^\pm(\mathbf{x}_R, \omega) = \frac{\omega^2}{4\pi^2}\int_{\mathbb{R}^2} \exp\{i\omega\mathbf{s}\cdot\mathbf{x}_{\mathrm{H},R}\}\tilde{p}^\pm(\mathbf{s}, x_{3,R}, \omega)\mathrm{d}\mathbf{s} \tag{A11}$$

and similar expressions for $a(\mathbf{x}_R,\omega)$ and $b(\mathbf{x}_R,\omega)$ but with the integration interval limited to $|\mathbf{s}| \le 1/c_0$, gives

$$b(\mathbf{x}_R,\omega) + \text{ evanescent waves} = p^+(\mathbf{x}_R,\omega), \tag{A12}$$

$$a(\mathbf{x}_R,\omega) + \text{ evanescent waves} = p^-(\mathbf{x}_R,\omega). \tag{A13}$$

Substitution of equations (A12) and (A13) into equation (10), ignoring the evanescent waves, gives equation (11).

A2 Analysis of the integral in equation (23)

We analyze the integral in equation (23). We show that we can transfer the operator $\partial_{3,R}$ from f to G^{s}, and that this is accompanied with a sign change. For a function of two space variables, $u(\mathbf{x}, \mathbf{x}_R, \omega)$, we define the spatial Fourier transform along the second space variable as

$$\tilde{u}(\mathbf{x}, \mathbf{s}, x_{3,R}, \omega) = \int_{\mathbb{R}^2} u(\mathbf{x}, \mathbf{x}_{\mathrm{H},R}, x_{3,R}, \omega)\exp\{i\omega\mathbf{s}\cdot\mathbf{x}_{\mathrm{H},R}\}\mathrm{d}\mathbf{x}_{\mathrm{H},R}. \tag{A14}$$

Note the opposite sign in the exponential, compared with that in equation (40). Using this Fourier transform and Parseval's theorem, we obtain for the integral in equation (23)

$$\begin{aligned} &\int_{\partial\mathbb{D}_R} \{\partial_{3,R} f(\mathbf{x}, \mathbf{x}_R, \omega)\} G^{\mathrm{s}}(\mathbf{x}_S, \mathbf{x}_R, \omega)\mathrm{d}\mathbf{x}_R = \\ &\frac{\omega^2}{4\pi^2}\int_{\mathbb{R}^2} \{\partial_{3,R}\tilde{f}(\mathbf{x}, -\mathbf{s}, x_{3,R}, \omega)\}\tilde{G}^{\mathrm{s}}(\mathbf{x}_S, \mathbf{s}, x_{3,R}, \omega)\mathrm{d}\mathbf{s}. \end{aligned} \tag{A15}$$

Note that $\tilde{f}(\mathbf{x},-\mathbf{s},x_{3,R},\omega)$ is differentiated with respect to the focal point depth $x_{3,R}$, hence, the one-way wave equation gets a sign opposite to that in equation (A4), i.e. $\partial_{3,R}\tilde{f}(\mathbf{x},-\mathbf{s},x_{3,R},\omega) = i\omega s_3\tilde{f}(\mathbf{x},-\mathbf{s},x_{3,R},\omega)$, with s_3 defined in equation (A5). We transfer $i\omega s_3$ to the Green's function and use $i\omega s_3\tilde{G}^{\mathrm{s}}(\mathbf{x}_S,\mathbf{s},x_{3,R},\omega) = -\partial_{3,R}\tilde{G}^{\mathrm{s}}(\mathbf{x}_S,\mathbf{s},x_{3,R},\omega)$ (which is a differentiation with respect to the source depth $x_{3,R}$). Making these substitutions in the right-hand side of equation (A15) and applying Parseval's theorem again gives

$$
\begin{aligned}
&-\frac{\omega^2}{4\pi^2}\int_{\mathbb{R}^2}\tilde{f}(\mathbf{x},-\mathbf{s},x_{3,R},\omega)\partial_{3,R}\tilde{G}^{\mathrm{s}}(\mathbf{x}_S,\mathbf{s},x_{3,R},\omega)\mathrm{d}\mathbf{s}\\
&=-\int_{\partial\mathbb{D}_R} f(\mathbf{x},\mathbf{x}_R,\omega)\partial_{3,R}G^{\mathrm{s}}(\mathbf{x}_S,\mathbf{x}_R,\omega)\mathrm{d}\mathbf{x}_R. \qquad \text{(A16)}
\end{aligned}
$$

Hence, we have transferred the operator $\partial_{3,R}$ under the integral in equation (23) from f to G^{s}, which involves a sign change.

APPENDIX B: DERIVATION OF THE ELASTODYNAMIC WAVE FIELD REPRESENTATION

B1 Derivation of the representation of equation (54)

We derive expressions for the coefficients $\mathbf{a}(\mathbf{x}_R,\omega)$ and $\mathbf{b}(\mathbf{x}_R,\omega)$ in the elastodynamic wave field representation of equation (53). We do this by formulating two boundary conditions at $\partial\mathbb{D}_R$. First, we consider the particle velocity vector $\mathbf{v}(\mathbf{x},\omega)$ at $\partial\mathbb{D}_R$. To this end, we evaluate equation (53) for $\mathbf{x}$ at $\partial\mathbb{D}_R$. Using the focusing condition formulated in equation (51) we thus obtain

$$
\begin{aligned}
\mathbf{v}(\mathbf{x},\omega)|_{x_3=x_{3,R}} &= \int_{\partial\mathbb{D}_R}\delta(\mathbf{x}_{\mathrm{H}}-\mathbf{x}_{\mathrm{H},R})\mathbf{a}(\mathbf{x}_R,\omega)\mathrm{d}\mathbf{x}_R+\int_{\partial\mathbb{D}_R}\delta(\mathbf{x}_{\mathrm{H}}-\mathbf{x}_{\mathrm{H},R})\mathbf{b}(\mathbf{x}_R,\omega)\mathrm{d}\mathbf{x}_R,\\
&= \{\mathbf{a}(\mathbf{x},\omega)+\mathbf{b}(\mathbf{x},\omega)\}_{x_3=x_{3,R}}. \qquad \text{(B1)}
\end{aligned}
$$

For the second boundary condition we analyze the traction vector $\boldsymbol{\tau}_3(\mathbf{x},\omega)$ at $\partial\mathbb{D}_R$. First we establish a relation between $\boldsymbol{\tau}_3(\mathbf{x},\omega)$ and $\mathbf{v}(\mathbf{x},\omega)$ in the homogeneous isotropic upper half-space, including $\partial\mathbb{D}_R$. Using equation (40), we transform $\mathbf{v}(\mathbf{x},\omega)$ and $\boldsymbol{\tau}_3(\mathbf{x},\omega)$ for $x_3\le x_{3,R}$ to $\tilde{\mathbf{v}}(\mathbf{s},x_3,\omega)$ and $\tilde{\boldsymbol{\tau}}_3(\mathbf{s},x_3,\omega)$, respectively. These fields can be related to vectors $\tilde{\mathbf{p}}^+$ and $\tilde{\mathbf{p}}^-$ containing downgoing and upgoing fields, respectively, according to

$$
\begin{pmatrix}-\tilde{\boldsymbol{\tau}}_3\\ \tilde{\mathbf{v}}\end{pmatrix}=\begin{pmatrix}\tilde{\mathbf{L}}_1^+ & \tilde{\mathbf{L}}_1^-\\ \tilde{\mathbf{L}}_2^+ & \tilde{\mathbf{L}}_2^-\end{pmatrix}\begin{pmatrix}\tilde{\mathbf{p}}^+\\ \tilde{\mathbf{p}}^-\end{pmatrix},\quad \text{for}\quad x_3\le x_{3,R}, \qquad \text{(B2)}
$$

(Kennett et al., 1978; Ursin, 1983; Wapenaar & Berkhout, 1989). We define the downgoing and upgoing parts of $\tilde{\mathbf{v}}$ as $\tilde{\mathbf{v}}^\pm=\tilde{\mathbf{L}}_2^\pm\tilde{\mathbf{p}}^\pm$ and rewrite equation (B2) as

$$
\begin{pmatrix}-\tilde{\boldsymbol{\tau}}_3\\ \tilde{\mathbf{v}}\end{pmatrix}=\begin{pmatrix}\tilde{\mathbf{D}}^+ & \tilde{\mathbf{D}}^-\\ \mathbf{I} & \mathbf{I}\end{pmatrix}\begin{pmatrix}\tilde{\mathbf{v}}^+\\ \tilde{\mathbf{v}}^-\end{pmatrix},\quad \text{for}\quad x_3\le x_{3,R}, \qquad \text{(B3)}
$$

with $\tilde{\mathbf{D}}^\pm=\tilde{\mathbf{L}}_1^\pm(\tilde{\mathbf{L}}_2^\pm)^{-1}$. The matrices $\tilde{\mathbf{L}}_1^\pm$ and $\tilde{\mathbf{L}}_2^\pm$ in equation (B2) are not uniquely defined. They depend on the chosen normalization of the fields contained in $\tilde{\mathbf{p}}^+$ and $\tilde{\mathbf{p}}^-$. However, independent of the normalization, the matrix $\tilde{\mathbf{D}}^\pm$ in equation (B3) is uniquely defined. It is given by

$$
\begin{aligned}
&\tilde{\mathbf{D}}^\pm(\mathbf{s}) = \qquad \text{(B4)}\\
&\frac{\rho c_S^2}{s_3^P s_3^S+\mathbf{s}\cdot\mathbf{s}}\begin{pmatrix}\pm((c_S^{-2}-s_2^2)s_3^P+s_2^2 s_3^S) & \pm s_1 s_2(s_3^P-s_3^S) & -s_1(c_S^{-2}-2(s_3^P s_3^S+\mathbf{s}\cdot\mathbf{s}))\\ \pm s_1 s_2(s_3^P-s_3^S) & \pm((c_S^{-2}-s_1^2)s_3^P+s_1^2 s_3^S) & -s_2(c_S^{-2}-2(s_3^P s_3^S+\mathbf{s}\cdot\mathbf{s}))\\ s_1(c_S^{-2}-2(s_3^P s_3^S+\mathbf{s}\cdot\mathbf{s})) & s_2(c_S^{-2}-2(s_3^P s_3^S+\mathbf{s}\cdot\mathbf{s})) & \pm s_3^S c_S^{-2}\end{pmatrix}
\end{aligned}
$$

with the vertical slownesses s_3^P and s_3^S for P- and S-waves, respectively, defined as

$$
s_3^{P,S}=\begin{cases}\sqrt{1/c_{P,S}^2-\mathbf{s}\cdot\mathbf{s}}, & \text{for } \mathbf{s}\cdot\mathbf{s}\le 1/c_{P,S}^2\\ i\sqrt{\mathbf{s}\cdot\mathbf{s}-1/c_{P,S}^2}, & \text{for } \mathbf{s}\cdot\mathbf{s}>1/c_{P,S}^2,\end{cases} \qquad \text{(B5)}
$$

where c_P and c_S are the P- and S-wave velocities, respectively, of the upper half-space $x_3 \leq x_{3,R}$. Applying the transform of equation (40) to equation (53) we obtain for $\mathbf{x}$ at $\partial\mathbb{D}_R$

$$\tilde{\mathbf{v}}(\mathbf{s}, x_{3,R}, \omega) = \int_{\partial\mathbb{D}_R} \tilde{\mathbf{F}}(\mathbf{s}, x_{3,R}, \mathbf{x}_R, \omega)\mathbf{a}(\mathbf{x}_R, \omega)\mathrm{d}\mathbf{x}_R + \int_{\partial\mathbb{D}_R} \tilde{\mathbf{F}}^*(-\mathbf{s}, x_{3,R}, \mathbf{x}_R, \omega)\mathbf{b}(\mathbf{x}_R, \omega)\mathrm{d}\mathbf{x}_R. \tag{B6}$$

Since $\tilde{\mathbf{F}}(\mathbf{s}, x_{3,R}, \mathbf{x}_R, \omega)$ is upgoing, the first term on the right-hand side is the upgoing velocity field $\tilde{\mathbf{v}}^-(\mathbf{s}, x_{3,R}, \omega)$ and the second term is, for propagating waves (i.e., for $\mathbf{s}\cdot\mathbf{s} \leq 1/c_P^2$), the downgoing velocity field $\tilde{\mathbf{v}}^+(\mathbf{s}, x_{3,R}, \omega)$. Hence, using equation (B3) we obtain for the transformed traction vector

$$\begin{aligned} -\tilde{\boldsymbol{\tau}}_3(\mathbf{s}, x_{3,R}, \omega) = \\ \tilde{\mathbf{D}}^-(\mathbf{s}) \int_{\partial\mathbb{D}_R} \tilde{\mathbf{F}}(\mathbf{s}, x_{3,R}, \mathbf{x}_R, \omega)\mathbf{a}(\mathbf{x}_R, \omega)\mathrm{d}\mathbf{x}_R \\ +\tilde{\mathbf{D}}^+(\mathbf{s}) \int_{\partial\mathbb{D}_R} \tilde{\mathbf{F}}^*(-\mathbf{s}, x_{3,R}, \mathbf{x}_R, \omega)\mathbf{b}(\mathbf{x}_R, \omega)\mathrm{d}\mathbf{x}_R, \end{aligned} \tag{B7}$$

for $\mathbf{s}\cdot\mathbf{s} \leq 1/c_P^2$ at $\partial\mathbb{D}_R$. Applying the transform of equation (40) to the focusing condition of equation (51) gives

$$\tilde{\mathbf{F}}(\mathbf{s}, x_{3,R}, \mathbf{x}_R, \omega) = \mathbf{I}\exp\{-i\omega\mathbf{s}\cdot\mathbf{x}_{\mathrm{H},R}\}. \tag{B8}$$

Substituting this into equation (B7) we obtain

$$-\tilde{\boldsymbol{\tau}}_3(\mathbf{s}, x_{3,R}, \omega) = \tilde{\mathbf{D}}^-(\mathbf{s})\tilde{\mathbf{a}}(\mathbf{s}, x_{3,R}, \omega) + \tilde{\mathbf{D}}^+(\mathbf{s})\tilde{\mathbf{b}}(\mathbf{s}, x_{3,R}, \omega), \tag{B9}$$

for $\mathbf{s}\cdot\mathbf{s} \leq 1/c_P^2$ at $\partial\mathbb{D}_R$. Combining this equation with the Fourier transform of equation (B1) yields

$$\begin{pmatrix} -\tilde{\boldsymbol{\tau}}_3 \\ \tilde{\mathbf{v}} \end{pmatrix}_{x_3=x_{3,R}} = \begin{pmatrix} \tilde{\mathbf{D}}^+ & \tilde{\mathbf{D}}^- \\ \mathbf{I} & \mathbf{I} \end{pmatrix} \begin{pmatrix} \tilde{\mathbf{b}} \\ \tilde{\mathbf{a}} \end{pmatrix}_{x_3=x_{3,R}}, \tag{B10}$$

for $\mathbf{s}\cdot\mathbf{s} \leq 1/c_P^2$ at $\partial\mathbb{D}_R$. Comparing this with equation (B3) we conclude

$$\tilde{\mathbf{b}}(\mathbf{s}, x_{3,R}, \omega) = \tilde{\mathbf{v}}^+(\mathbf{s}, x_{3,R}, \omega), \tag{B11}$$

$$\tilde{\mathbf{a}}(\mathbf{s}, x_{3,R}, \omega) = \tilde{\mathbf{v}}^-(\mathbf{s}, x_{3,R}, \omega), \tag{B12}$$

for $\mathbf{s}\cdot\mathbf{s} \leq 1/c_P^2$ at $\partial\mathbb{D}_R$. Transforming these expressions back to the space domain gives

$$\mathbf{b}(\mathbf{x}_R, \omega) + \text{evanescent waves} = \mathbf{v}^+(\mathbf{x}_R, \omega), \tag{B13}$$

$$\mathbf{a}(\mathbf{x}_R, \omega) + \text{evanescent waves} = \mathbf{v}^-(\mathbf{x}_R, \omega). \tag{B14}$$

Substitution of equations (B13) and (B14) into equation (53), ignoring the evanescent waves, gives equation (54).

B2 Derivation of the modified elastodynamic Green's function

We derive a modified elastodynamic Green's function $\boldsymbol{\Gamma}(\mathbf{x}, \mathbf{x}_S, \omega)$, such that for $\mathbf{x}$ at $\partial\mathbb{D}_R$, i.e., just below the source, the downgoing part of $\boldsymbol{\Gamma}(\mathbf{x}, \mathbf{x}_S, \omega)$ obeys equation (58), i.e.,

$$\lim_{x_3 \downarrow x_{3,S}} \boldsymbol{\Gamma}^+(\mathbf{x}, \mathbf{x}_S, \omega) = \mathbf{I}\delta(\mathbf{x}_\mathrm{H} - \mathbf{x}_{\mathrm{H},S}). \tag{B15}$$

To this end we first investigate the properties of the downgoing part of $\mathbf{G}(\mathbf{x}, \mathbf{x}_S, \omega)$ defined in equations (56) and (57), just below the source. Consider the inverse of equation (B3)

$$\begin{pmatrix} \tilde{\mathbf{v}}^+ \\ \tilde{\mathbf{v}}^- \end{pmatrix} = \begin{pmatrix} (\tilde{\mathbf{D}}^+ - \tilde{\mathbf{D}}^-)^{-1} & (\mathbf{I} - (\tilde{\mathbf{D}}^-)^{-1}\tilde{\mathbf{D}}^+)^{-1} \\ (\tilde{\mathbf{D}}^- - \tilde{\mathbf{D}}^+)^{-1} & (\mathbf{I} - (\tilde{\mathbf{D}}^+)^{-1}\tilde{\mathbf{D}}^-)^{-1} \end{pmatrix} \begin{pmatrix} -\tilde{\boldsymbol{\tau}}_3 \\ \tilde{\mathbf{v}} \end{pmatrix}, \quad \text{for} \quad x_3 \leq x_{3,R}. \tag{B16}$$

The upper-left matrix, $(\tilde{\mathbf{D}}^+ - \tilde{\mathbf{D}}^-)^{-1}$, gives the relation between $-\tilde{\boldsymbol{\tau}}_3$ and the downgoing velocity vector $\tilde{\mathbf{v}}^+$. The same matrix transforms a unit force source in a homogeneous half-space into the downgoing part of the Green's

function just below this source, hence (defining $\tilde{\mathbf{D}} = \tilde{\mathbf{D}}^+ - \tilde{\mathbf{D}}^-$)

$$\lim_{x_3 \downarrow x_{3,S}} \tilde{\mathbf{G}}^+(\mathbf{s}, x_3, \mathbf{0}, x_{3,S}, \omega) = \tilde{\mathbf{D}}^{-1}(\mathbf{s}) = \\ \frac{1}{2\rho} \begin{pmatrix} \frac{s_1^2}{s_3^P} + \left(\frac{1}{c_S^2} - s_1^2\right)\frac{1}{s_3^S} & \left(\frac{1}{s_3^P} - \frac{1}{s_3^S}\right) s_1 s_2 & 0 \\ \left(\frac{1}{s_3^P} - \frac{1}{s_3^S}\right) s_1 s_2 & \frac{s_2^2}{s_3^P} + \left(\frac{1}{c_S^2} - s_2^2\right)\frac{1}{s_3^S} & 0 \\ 0 & 0 & s_3^P + \frac{\mathbf{s}\cdot\mathbf{s}}{s_3^S} \end{pmatrix}. \tag{B17}$$

In equation (B17) the source is located at $(\mathbf{0}, x_{3,S})$. Next, we consider $\mathbf{G}(\mathbf{x}, \mathbf{x}_S, \omega)$ for a laterally shifted source position $(\mathbf{x}_{\mathrm{H},S}, x_{3,S})$. Applying a spatial Fourier transform along the horizontal source coordinate $\mathbf{x}_{\mathrm{H},S}$, using equation (A14) with $\mathbf{x}_{\mathrm{H},R}$ replaced by $\mathbf{x}_{\mathrm{H},S}$, yields $\tilde{\mathbf{G}}(\mathbf{x}, \mathbf{s}, x_{3,S}, \omega)$. For the downgoing part just below the source we obtain a phase-shifted version of the Green's function of equation (B17), according to

$$\lim_{x_3 \downarrow x_{3,S}} \tilde{\mathbf{G}}^+(\mathbf{x}, \mathbf{s}, x_{3,S}, \omega) \quad = \quad \tilde{\mathbf{D}}^{-1}(\mathbf{s}) \exp\{i\omega \mathbf{s} \cdot \mathbf{x}_{\mathrm{H}}\}. \tag{B18}$$

Comparing this with the desired condition of equation (B15) suggests to define the modified Green's function (for arbitrary $\mathbf{x}$) as

$$\tilde{\mathbf{\Gamma}}(\mathbf{x}, \mathbf{s}, x_{3,S}, \omega) = \tilde{\mathbf{G}}(\mathbf{x}, \mathbf{s}, x_{3,S}, \omega) \tilde{\mathbf{D}}(\mathbf{s}), \tag{B19}$$

such that

$$\lim_{x_3 \downarrow x_{3,S}} \tilde{\mathbf{\Gamma}}^+(\mathbf{x}, \mathbf{s}, x_{3,S}, \omega) = \mathbf{I} \exp\{i\omega \mathbf{s} \cdot \mathbf{x}_{\mathrm{H}}\}. \tag{B20}$$

The inverse Fourier transform from $\mathbf{s}$ to $\mathbf{x}_{\mathrm{H},S}$ gives equation (B15).

We define the reflection response $\tilde{\mathbf{R}}(\mathbf{x}_R, \mathbf{s}, x_{3,S}, \omega)$ of the medium below $\partial\mathbb{D}_R$ as the upgoing part of the modified Green's function $\tilde{\mathbf{\Gamma}}(\mathbf{x}_R, \mathbf{s}, x_{3,S}, \omega)$, with $\mathbf{x}_R$ at $\partial\mathbb{D}_R$, hence

$$\tilde{\mathbf{R}}(\mathbf{x}_R, \mathbf{s}, x_{3,S}, \omega) \quad = \quad \tilde{\mathbf{\Gamma}}^-(\mathbf{x}_R, \mathbf{s}, x_{3,S}, \omega), \tag{B21}$$

or, using equation (B19),

$$\begin{aligned} \tilde{\mathbf{R}}(\mathbf{x}_R, \mathbf{s}, x_{3,S}, \omega) \quad &= \quad \tilde{\mathbf{G}}^-(\mathbf{x}_R, \mathbf{s}, x_{3,S}, \omega) \tilde{\mathbf{D}}(\mathbf{s}) \\ &= \quad \tilde{\mathbf{G}}^{\mathrm{s}}(\mathbf{x}_R, \mathbf{s}, x_{3,S}, \omega) \tilde{\mathbf{D}}(\mathbf{s}), \end{aligned} \tag{B22}$$

where superscript s stands for scattered. The inverse Fourier transform of equation (B21) from $\mathbf{s}$ to $\mathbf{x}_{\mathrm{H},S}$ yields equation (59).

B3 Derivation of the representation of equation (61)

To obtain a representation for $\mathbf{G}(\mathbf{x}, \mathbf{x}_S, \omega)$ we start by transforming all terms in equation (60) along $\mathbf{x}_{\mathrm{H},S}$, using equation (A14), with $\mathbf{x}_{\mathrm{H},R}$ replaced by $\mathbf{x}_{\mathrm{H},S}$, hence

$$\tilde{\mathbf{\Gamma}}(\mathbf{x}, \mathbf{s}, x_{3,S}, \omega) \quad = \quad \int_{\partial\mathbb{D}_R} \mathbf{F}(\mathbf{x}, \mathbf{x}_R, \omega) \tilde{\mathbf{R}}(\mathbf{x}_R, \mathbf{s}, x_{3,S}, \omega) \mathrm{d}\mathbf{x}_R + \tilde{\mathbf{F}}^*(\mathbf{x}, -\mathbf{s}, x_{3,S}, \omega), \\ \text{for} \quad x_3 \geq x_{3,R}. \tag{B23}$$

We introduce a modified focusing function $\tilde{\mathbf{f}}(\mathbf{x}, \mathbf{s}, x_{3,S}, \omega)$ via

$$\tilde{\mathbf{F}}(\mathbf{x}, \mathbf{s}, x_{3,S}, \omega) = \tilde{\mathbf{f}}(\mathbf{x}, \mathbf{s}, x_{3,S}, \omega) \tilde{\mathbf{D}}(\mathbf{s}). \tag{B24}$$

According to equation (B17) we have for propagating waves (i.e., for $\mathbf{s} \cdot \mathbf{s} \leq 1/c_P^2$)

$$\tilde{\mathbf{D}}(\mathbf{s}) = \tilde{\mathbf{D}}(-\mathbf{s}) = \tilde{\mathbf{D}}^*(\mathbf{s}) = \tilde{\mathbf{D}}^t(\mathbf{s}). \tag{B25}$$

Hence, for $\tilde{\mathbf{F}}^*(\mathbf{x}, -\mathbf{s}, x_{3,S}, \omega)$ we obtain, analogous to equation (B19),

$$\tilde{\mathbf{F}}^*(\mathbf{x}, -\mathbf{s}, x_{3,S}, \omega) = \tilde{\mathbf{f}}^*(\mathbf{x}, -\mathbf{s}, x_{3,S}, \omega) \tilde{\mathbf{D}}(\mathbf{s}). \tag{B26}$$

Multiplying all terms in equation (B23) from the right by $\tilde{\mathbf{D}}^{-1}(\mathbf{s})$, using equations (B19), (B22) and (B26), and transforming the resulting expression back from $\mathbf{s}$ to $\mathbf{x}_{\mathrm{H},S}$ gives

$$\mathbf{G}(\mathbf{x},\mathbf{x}_S,\omega) \quad = \quad \int_{\partial\mathbb{D}_R} \mathbf{F}(\mathbf{x},\mathbf{x}_R,\omega)\mathbf{G}^{\mathrm{s}}(\mathbf{x}_R,\mathbf{x}_S,\omega)\mathrm{d}\mathbf{x}_R + \mathbf{f}^{*}(\mathbf{x},\mathbf{x}_S,\omega), \quad \text{for} \quad x_3 \geq x_{3,R}. \tag{B27}$$

We modify the integral step by step. First we use source-receiver reciprocity for the scattered Green's function $\mathbf{G}^{\mathrm{s}}(\mathbf{x}_R,\mathbf{x}_S,\omega)$ and we apply Parseval's theorem. We thus obtain for the integral in equation (B27)

$$\frac{\omega^2}{4\pi^2}\int_{\mathbb{R}^2} \tilde{\mathbf{F}}(\mathbf{x},-\mathbf{s},x_{3,R},\omega)\{\tilde{\mathbf{G}}^{\mathrm{s}}(\mathbf{x}_S,\mathbf{s},x_{3,R},\omega)\}^t\mathrm{d}\mathbf{s}. \tag{B28}$$

Substituting equation (B24), using equation (B25), gives

$$\frac{\omega^2}{4\pi^2}\int_{\mathbb{R}^2} \tilde{\mathbf{f}}(\mathbf{x},-\mathbf{s},x_{3,R},\omega)\{\tilde{\mathbf{G}}^{\mathrm{s}}(\mathbf{x}_S,\mathbf{s},x_{3,R},\omega)\tilde{\mathbf{D}}(\mathbf{s})\}^t\mathrm{d}\mathbf{s}. \tag{B29}$$

Using equation (B22) this gives

$$\frac{\omega^2}{4\pi^2}\int_{\mathbb{R}^2} \tilde{\mathbf{f}}(\mathbf{x},-\mathbf{s},x_{3,R},\omega)\{\tilde{\mathbf{R}}(\mathbf{x}_S,\mathbf{s},x_{3,R},\omega)\}^t\mathrm{d}\mathbf{s}. \tag{B30}$$

Applying Parseval's theorem again and inserting the integral in equation (B27) yields equation (61). It has been derived without applying decomposition in the lower half-space, but it excludes the contribution from waves that are evanescent at $\partial\mathbb{D}_R$.

REFERENCES

Berkhout, A. J., 1982. *Seismic Migration. Imaging of acoustic energy by wave field extrapolation. A. Theoretical aspects*, Elsevier.

Berryhill, J. R., 1984. Wave-equation datuming before stack, *Geophysics*, **49**, 2064–2066.

Brackenhoff, J., Thorbecke, J., & Wapenaar, K., 2019. Monitoring of induced distributed double-couple sources using Marchenko-based virtual receivers, *Solid Earth*, **10**, 1301–1319.

Broggini, F. & Snieder, R., 2012. Connection of scattering principles: a visual and mathematical tour, *European Journal of Physics*, **33**, 593–613.

Burridge, R., 1980. The Gelfand-Levitan, the Marchenko, and the Gopinath-Sondhi integral equations of inverse scattering theory, regarded in the context of inverse impulse-response problems, *Wave Motion*, **2**, 305–323.

Corones, J. P., 1975. Bremmer series that correct parabolic approximations, *J. Math. Anal. Appl.*, **50**, 361–372.

Curtis, A. & Halliday, D., 2010. Source-receiver wavefield interferometry, *Physical Review E*, **81**, 046601.

da Costa Filho, C. A., Ravasi, M., Curtis, A., & Meles, G. A., 2014. Elastodynamic Green's function retrieval through single-sided Marchenko inverse scattering, *Physical Review E*, **90**, 063201.

Diekman, L. & Vasconcelos, I., 2021. Focusing and Green's function retrieval in three-dimensional inverse scattering revisited: a single-sided Marchenko integral for the full wave field, *Physical Review Research*, **3**, in press.

Elison, P., Dukalski, M. S., de Vos, K., van Manen, D. J., & Robertsson, J. O. A., 2020. Data-driven control over short-period internal multiples in media with a horizontally layered overburden, *Geophysical Journal International*, **221**, 769–787.

Fishman, L. & McCoy, J. J., 1984. Derivation and application of extended parabolic wave theories. I. The factorized Helmholtz equation, *J. Math. Phys.*, **25**(2), 285–296.

Halliday, D., Curtis, A., & Wapenaar, K., 2012. Generalized PP + PS = SS from seismic interferometry, *Geophysical Journal International*, **189**, 1015–1024.

Hokstad, K., 2000. Multicomponent Kirchhoff migration, *Geophysics*, **65**(3), 861–873.

Holicki, M., Drijkoningen, G., & Wapenaar, K., 2019. Acoustic directional snapshot wavefield decomposition, *Geophysical Prospecting*, **67**, 32–51.

Jia, X., Guitton, A., & Snieder, R., 2018. A practical implementation of subsalt Marchenko imaging with a Gulf of Mexico data set, *Geophysics*, **83**(5), S409–S419.

Kennett, B. L. N., Kerry, N. J., & Woodhouse, J. H., 1978. Symmetries in the reflection and transmission of elastic waves, *Geophysical Journal of the Royal Astronomical Society*, **52**, 215–230.

Kiraz, M. S. R., Snieder, R., & Wapenaar, K., 2020. Marchenko focusing without up/down decomposition, in *SEG, Expanded Abstracts*, pp. 3593–3597.

Liu, F., Zhang, G., Morton, S. A., & Leveille, J. P., 2011. An effective imaging condition for reverse-time migration using wavefield decomposition, *Geophysics*, **76**, S29–S39.

Lomas, A. & Curtis, A., 2019. An introduction to Marchenko methods for imaging, *Geophysics*, **84**(2), F35–F45.

Mildner, C., Broggini, F., de Vos, K., & Robertsson, J. O. A., 2019. Accurate source wavelet estimation using Marchenko focusing functions, *Geophysics*, **84**(6), Q73–Q88.

Oristaglio, M. L., 1989. An inverse scattering formula that uses all the data, *Inverse Problems*, **5**, 1097–1105.

Pereira, R., Ramzy, M., Griscenco, P., Huard, B., Huang, H., Cypriano, L., & Khalil, A., 2019. Internal multiple attenuation for OBN data with overburden/target separation, in *SEG, Expanded Abstracts*, pp. 4520–4524.

Porter, R. P., 1970. Diffraction-limited, scalar image formation with holograms of arbitrary shape, *Journal of the Optical Society of America*, **60**, 1051–1059.

Ravasi, M. & Vasconcelos, I., 2020. On the implementation of large-scale integral operators with modern HPC solutions – Application to 3D Marchenko imaging by least-squares inversion, *arXiv:2011.11120*.

Ravasi, M., Vasconcelos, I., Kritski, A., Curtis, A., da Costa Filho, C. A., & Meles, G. A., 2016. Target-oriented Marchenko imaging of a North Sea field, *Geophysical Journal International*, **205**, 99–104.

Reinicke, C. & Wapenaar, K., 2019. Elastodynamic single-sided homogeneous Green's function representation: Theory and numerical examples, *Wave Motion*, **89**, 245–264.

Reinicke, C., Dukalski, M., & Wapenaar, K., 2020. Comparison of monotonicity challenges encountered by the inverse scattering series and the Marchenko demultiple method for elastic waves, *Geophysics*, **85**(5), Q11–Q26.

Schoenberg, M. & Sen, P. N., 1983. Properties of a periodically stratified acoustic half-space and its relation to a Biot fluid, *Journal of the Acoustical Society of America*, **73**, 61–67.

Singh, S. & Snieder, R., 2017. Source-receiver Marchenko redatuming: Obtaining virtual receivers and virtual sources in the subsurface, *Geophysics*, **82**(3), Q13–Q21.

Slob, E., Wapenaar, K., Broggini, F., & Snieder, R., 2014. Seismic reflector imaging using internal multiples with Marchenko-type equations, *Geophysics*, **79**(2), S63–S76.

Staring, M. & Wapenaar, K., 2020. Three-dimensional Marchenko internal multiple attenuation on narrow azimuth streamer data of the Santos Basin, Brazil, *Geophysical Prospecting*, **68**, 1864–1877.

Staring, M., Pereira, R., Douma, H., van der Neut, J., & Wapenaar, K., 2018. Source-receiver Marchenko redatuming on field data using an adaptive double-focusing method, *Geophysics*, **83**(6), S579–S590.

Stoffa, P. L., 1989. *Tau-p - A plane wave approach to the analysis of seismic data*, Kluwer Academic Publishers, Dordrecht.

Ursin, B., 1983. Review of elastic and electromagnetic wave propagation in horizontally layered media, *Geophysics*, **48**, 1063–1081.

Van der Neut, J., Johnson, J. L., van Wijk, K., Singh, S., Slob, E., & Wapenaar, K., 2017. A Marchenko equation for acoustic inverse source problems, *Journal of the Acoustical Society of America*, **141**(6), 4332–4346.

Wapenaar, C. P. A. & Berkhout, A. J., 1989. *Elastic wave field extrapolation*, Elsevier, Amsterdam.

Wapenaar, K., 2020. The Marchenko method for evanescent waves, *Geophysical Journal International*, **223**, 1412–1417.

Wapenaar, K. & Slob, E., 2014. On the Marchenko equation for multicomponent single-sided reflection data, *Geophysical Journal International*, **199**, 1367–1371.

Wapenaar, K., Broggini, F., Slob, E., & Snieder, R., 2013. Three-dimensional single-sided Marchenko inverse scattering, data-driven focusing, Green's function retrieval, and their mutual relations, *Physical Review Letters*, **110**, 084301.

Wapenaar, K., Thorbecke, J., van der Neut, J., Broggini, F., Slob, E., & Snieder, R., 2014. Marchenko imaging, *Geophysics*, **79**(3), WA39–WA57.

Wapenaar, K., Thorbecke, J., & van der Neut, J., 2016a. A single-sided homogeneous Green's function representation for holographic imaging, inverse scattering, time-reversal acoustics and interferometric Green's function retrieval, *Geophysical Journal International*, **205**, 531–535.

Wapenaar, K., van der Neut, J., & Slob, E., 2016b. Unified double- and single-sided homogeneous Green's function representations, *Proceedings of the Royal Society A*, **472**, 20160162.

Yoon, K. & Marfurt, K. J., 2006. Reverse-time migration using the Poynting vector, *Exploration Geophysics*, **37**,

102–107.

Zhang, L. & Slob, E., 2020. A fast algorithm for multiple elimination and transmission compensation in primary reflections, *Geophysical Journal International*, **221**, 371–377.